Electrical Conduction Transport Mechanisms of Barium Titanate-Based Multilayer Ceramic Capacitors

by

Tong Zhang

Thesis submitted to the Faculty of the
Virginia Polytechnic Institute and State University
in partial fulfillment of the requirements for the degree of
Master of Science
in
Materials Engineering

APPROVED:

Larry C. Burton, Chairman

Richard H. Zallen

Shinzo Onishi

August, 1988

Blacksburg, Virginia

Electrical Conduction Transport Mechanisms of Barium Titanate-Based Multilayer Ceramic Capacitors

by

Tong Zhang

Larry C. Burton, Chairman

Materials Engineering

(ABSTRACT)

The major objectives of this study were to examine electrical conduction properties of $BaTiO_3$-based multilayer ceramic (MLC) capacitors in order to gain a better understanding of the conduction transport mechanisms inside the devices. The experiments involved mainly leakage current versus time measurements under both low temperature-low voltage stress and high temperature-high voltage stress.

It was established that leakage current conduction in a MLC capacitor under temperature-voltage stress can be divided into three different conduction regions due to different mechanisms. Those regions are polarization current, DC conduction current and degradation current. The polarization current decreases with time as a power law relation, i.e. $I_C(t) \propto t^{-m}$ where the exponent value m is strongly dependent on the type of capacitor and temperature, but is only weakly dependent on the applied voltage.

It has been proposed that two degradation models (a charge carrier concentration model and a reduction of grain

boundary barrier height model) can explain the degradation behavior for the Z5U devices tested. Degradation measurements indicate that the lifetime for Z5U capacitors can be described by Minford's expression. However, these models account only partly for X7R degradation. X7R behavior is characterized by an early power law time dependence, followed by exponential voltage dependence.

The most probable conduction transport mechanism in X7R capacitors is small polaron hopping, while grain boundary transmission may be the predominant conduction transport mechanism in Z5U capacitors.

ACKNOWLEDGEMENTS

The author wishes to express his sincere appreciation to his advisor Dr. Larry C. Burton for his guidance, his support and his endless amount of patience. Special thanks go to his other committee members, Dr. Richard H. Zallen and Dr. Shinzo Onishi for their review and suggestions.

The author would like to extend sincerest thanks to his friends and colleagues in Electronic Materials Laboratory, P. Johnson, S. Sen, E. Ellis, A. Vaseashta, C. Turman, I.K. Yoo, R. Reddy, E. Cole, Y. Hwang, S. Villamil and C.J. Chen, who provided both friendship and assistance during the course of his study. Mrs. K. Rohr in Materials Engineering Department is acknowledged for help with the microscopic pictures.

The Office of Naval Research is also acknowledged for the financial support of this work.

The author also wishes to express the utmost thanks to his wife, , for making the work for this project easier than it could have been through extreme amounts of encouragement, love, patience, thoughtfulness and understanding.

TABLE OF CONTENTS

LIST OF ILLUSTRATIONS

LIST OF TABLES

Chapter 1: INTRODUCTION

Multilayer ceramic capacitors are mostly produced and used in the United States. Compared to a single thickness ceramic capacitor, a multilayer construction affords greater capacitance density at the cost of lower operating voltage. The small multilayer units (or chips) are manufactured to be physically compatible with the solid-state semiconductor components in hybrid circuits. They are also used as monolithic encapsulated capacitors for reducing the circuit size in cases where the low-voltage rating is not of consequence.

Ceramic capacitors have been grounded into different categories by the Electronic Industries Association in the United States[79], as shown in Table 1.

Class 1 capacitors have relatively low capacitance with low dielectric loss, a low temperature coefficient of the capacitance, and low rate of aging of the capacitance value. For barium titanate based ceramic capacitors in Class 1, a very low proportion of $BaTiO_3$ results in low or medium dielectric constant (K) per unit volume. Class 1 capacitors do not display ferroelectric characteristics. NPO (COG) multilayer ceramic capacitors are categorized as Class 1 devices. This type of capacitor was originally based on rutile (TiO_2), but now tends to contain 15 percent to at most 49 percent $BaTiO_3$. It is to be noted that this type of

multilayer ceramic (MLC) capacitor has relatively stable characteristics as indicated in Table 3.

Class 2 capacitors are produced using a greater proportion of barium titanate and other high permittivity materials. X7R and Z5U MLC capacitors are high-K Class 2 capacitors. A typical X7R composition contains 85 to 97 percent $BaTiO_3$ while a Z5U mix has in general 65 to 90 percent $BaTiO_3$ [78]. These high-K MLC capacitors are unstable and tend to age because of the ferroelectric nature of these devices. The Z5U dielectrics, with K value of about 5000, are more unstable than X7R with K value about 2000.

Besides aging (aging of both capacitance value and loss angle tan δ value), high-K MLC capacitors degrade under voltage-temperature stress after a certain operating period. The degradation in use causes failure of the devices. These factors result in instabilities and limit the use of Class 2 high-K ceramic capacitors. This is particularly true in high reliability applications such as the military, where operations are severe. It is essential to clearly understand the relaxation mechanisms in dielectrics because the present perception of aging is primarily on the relaxation of mechanical stresses [78,80]. Much work has been carried out on the phenomena of dielectric relaxation[4,14,80]. However, the degradation mechanism has not been well understood because of the complicated microstructural changes due to the charge

carrier transport in ceramics. The degradation of multilayer ceramic capacitors manifests itself in the form of increased leakage current. It is, therefore, necessary to specifically define what contributes and controls electrical conduction in these devices.

The conductivity behavior of dielectrics is of particular importance in the case of barium titanate. It has a cubic perovskite type structure and is the prototype material of most ceramic dielectrics. $BaTiO_3$ has a band gap about 3.2 eV [78] and is intrinsically a good insulator. However, its crystal structure lends itself to several varieties of defects, any of which can lead to higher electrical conduction. The charge carriers are usually n-type. There also exist the oxygen vacancies. The vacancies are either due to the dissociation at elevated processing temperatures, or may be due to the presence of allovalent acceptor dopants in the ceramic. The allovlant acceptor may result from raw material impurities or processing, or both.

Degradation is defined as the increase in leakage current with time due to a decrease in the resistance of the material. Grain, grain boundaries and electrode contacts can all contribute, to some extent and in some form, to the ceramic resistance. The relative role of the resistance components and different conduction mechanisms such as hopping transport in grains and the thermionic emission at the grain boundaries, etc., need to be determined

experimentally. Thus, a better understanding of the factors that influence the resistance of high resistance, high dielectric constant ceramic is required in order to achieve the following:

a) improve capacitor processing techniques,

b) select materials for use in devices,

c) enhance lifetime by decreasing the leakage conduction.

Chapter 2: RESEARCH OBJECTIVES

Conduction mechanisms in high K and high resistivity multilayer ceramic capacitors are still not well understood. The dominant leakage current charge carrier in multilayer ceramic (MLC) capacitors, and its mode of transport, have not been well established. The main objective of this research is to obtain a better understanding of the mode of the transport of charge carriers under different temperature-voltage stresses in $BaTiO_3$-based MLC capacitors. This is achieved by the use of electrical conduction testing techniques.

The essential methods are to measure, compare and model Z5U and X7R MLC capacitor leakage currents for short and long times over a wide range of accelerated conditions. Several questions related to this objective were addressed:

(1) What is the dominant conduction process for MLC capacitors under operating conditions?

(2) What are the sources of the charge carriers? Are they bulk carriers already presented in the material, injected carriers from electrodes, or other type of carriers generated under stress?

(3) What is the carrier transport mode? Does it change

with certain parameters such as time, temperature and applied voltage?

(4) How do the leakage currents change with time in degradation?

(5) How does degradation behavior for Z5U and X7R capacitors agree with the degradation models that have been reported?

It was felt that by answering these questions, significant information would be available with regard to the predominant charge carrier transport processes in the MLC capacitors. The questions were approached by means of the following:

(1) leakage current versus time measurements for several types of capacitors in the temperature-voltage range defined in the manufacturers specifications, or higher temperature-voltage stresses;

(2) time dependence of capacitance and charge-discharge currents;

(3) current-voltage characteristics for commercial Z5U

and X7R MLC capacitors;

(4) leakage current measurements for long times, over a wide range of accelerated conditions, and

(5) theoretical models compared to experimental results of degradation for both Z5U and X7R MLC capacitors.

Chapter 3 : LITERATURE REVIEW

Electrical conduction transport in multilayer ceramic capacitors is a very important phenomenon in the context of capacitor lifetime. The leakage currents in $BaTiO_3$-based MLC capacitors are attributed to the concentration of predominant charge carriers and the mode of their transport. Generally, the lower the leakage current, the longer is the capacitor lifetime. The magnitude of the leakage current is affected by various factors such as material composition, grain size, grain shape, density of dopant, defects, electrode material, dielectric layer and electrode geometry, etc.

This review emphasizes the known theoretical and experimental results, the models, and assumptions corresponding to conduction transport phenomena.

3.1 Polarization in Dielectrics

Consider to start with a homogeneous dielectric, consisting of an ensemble of polarizable units which may be atoms, ions, molecules, unit cells, macromolecular chains or crystallites. The relationship between the polarization $\vec{P}$ and the Lorentz field $\vec{E}_L$ is given by

$$\vec{P} = \sum_i N_i \alpha_i \vec{E}_{Li} \qquad \text{------- (3.1)}$$

where N_i is the density of i type unit, α_i is the polarizability of i type unit and E_{Li} is the Lorentz field for i type unit. The above relationship is correct only for those polarizable units whose dimensions are negligible relative to the macroscopic dimensions. In this case, the macroscopic polarizability coincides with the electrical susceptibility[48] which are represented as:

$$\sum_i N_i \alpha_i = \alpha = \chi \qquad \text{(CGS)}$$

Consequently Eqn.(3.1) becomes

$$\vec{P} = \sum_i N_i \alpha_i \vec{E} = \alpha \vec{E} \qquad \text{--------(3.2)}$$

The overall polarizability, α , of a monocrystalline dielectric is made up of three terms to which two more are added for polycrystalline and ferroelectric materials:

$$\alpha = \alpha_e + \alpha_i + \alpha_d + \alpha_b + \alpha_f \qquad \text{-------(3.3)}$$

The following are the principal sources of polarizability:

α_e , electronic, due to the displacement of the electron cloud relative to the nucleus of the atom.

α_i , ionic, due to the displacement of ions in an electric field from equilibrium positions, and the accompanying displacements of their electron clouds.

α_d , is due to the localized charge movements that possess a permanent dipole moment and to the rotation of dipoles in polar covalent solids.

α_b , is the characteristic of polycrystalline materials which contain mobile charges. In an electric field, polarization may arise due to the accumulation of mobile charges on a crystalline surface. This accumulation is favored by the grain boundaries or by the second phase, both of which act as barriers against the motion of charge carriers.

α_f , is due to the co-operative change in direction of dipoles in the domain of ferroelectric materials.

α_i, α_d and α_e are the most important contributors to the permittivity in ferroelectric ceramics. For high-K dielectric ceramics, another polarization contributor, charge carrier hopping, should be considered[4,49]. This has a very important role in polarization, direct current and dielectric loss.

There are hopping charge carriers which are characterized by the fact that they spend most of the time in localized sites where they are subjected only to relatively small thermal vibrations. But occasionally they make a big jump or a hopping transition to some neighboring localized sites which may be one or many atomic spacings away. The probability of a hopping transition may be determined by the combined effect of the distance between

the two sites and the potential barriers that have to be overcome. The transition may be a thermally assisted hop over the potential barrier or a tunnelling transition through the barrier - the latter requiring negligible activation energy. The hopping process gives rise to direct current conduction but may, under certain boundary conditions, lead to polarization.

In strongly disordered solids the normal concept of band conduction by free carriers does not apply. It is suggested that electrons become localized and can only move by hopping between localized sites. A many-body universal model of dielectric relaxation was originally proposed by Jonscher[4,50]. In this model, because a dielectric system is necessarily disordered, there exist strong interactions that result in high probability of configurational tunnelling by dipoles or charge particles. Hence, there is not any need for these transitions to be thermally excited. This process is a small transition and is due to the mutual slight rearrangements of carriers in a disordered system.

In an otherwise ordered array with defects, the hopping motion requires energy typically of the order of 1 eV[50] to take the charge carriers over the potential barrier hindering its motion in the lattice. This process is thermally activated and is called a large transition. It results in steady state direct current from ionic or electronic transport.

Fig.1 shows a potential energy diagram of a many-body two-level system representing the energy of a large number of interacting system. The two wells correspond to the preferred positions or orientations of dipoles or carriers. The splitting of the bottoms by $2B_{eff}$ is shown. The shaded regions represent the energy state of width 2ξ resulting from particle interactions. The transitions a and b correspond to the large transitions over the barrier height ΔE, with thermal excitation in case a and with particle tunnelling in case b. Transitions c and d are configurational tunnelling small transitions of the flip and flip-flop types, respectively. They do not involve thermal assistance and are only dependent on the number of interactions. Both the flip and thermally excited large transitions cause a relaxation of the dipole movement. However, in real dielectric systems all three types of transitions take place at all times, although at different relative rates.

3.2 Degradation

It is evident that degradation of insulation resistance is the primary failure mechanism of high-K multilayer ceramic[6,17], and of thick-film and thin film capacitors[15,26]. The degradation of the insulation resistance can result in the increase of leakage current

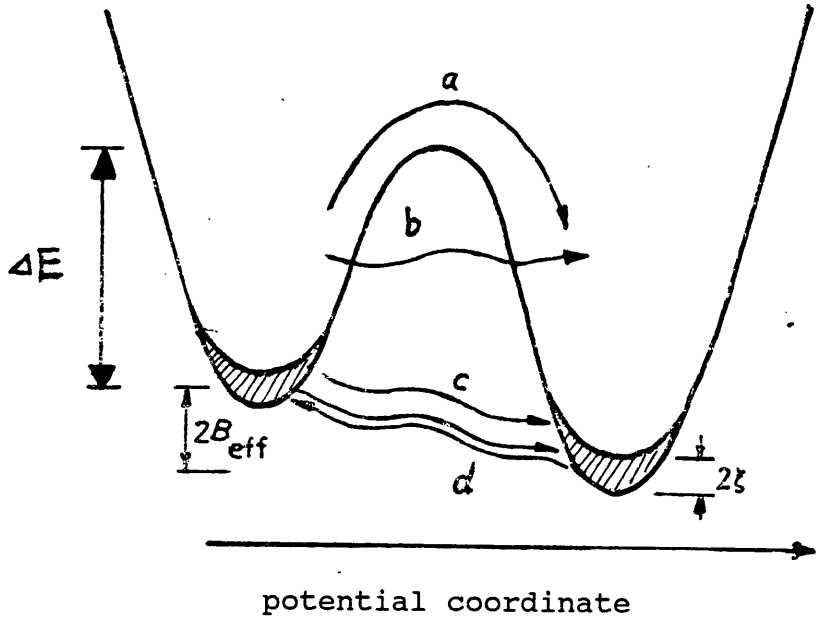

Figure 1. The double potential wells for the two-level model representing the energy of a large number of individual systems in an interactive dielectric material. [taken from (59)]

with time. The degradation rate is dependent the on applied voltage, temperature and dielectric thickness[7]. These are the primary factors affecting the leakage current. The degradation leakage current is measured under accelerated temperature and voltage conditions.

The temperature dependence of current can be expressed by

$$I = I_o \exp(-E_A/kT) \quad \text{-------} \quad (3.4)$$

where E_A is the activation energy[10]. This activation energy may be due to oxygen ion diffusion, polaron hopping transport, grain boundary barrier transport, Schottky barrier height or thermal activation energy of a deep donor. Either a reduction of E_A, or increasing temperature will result in an increase in the degradation[7,12]. It has been verified by thermoelectric and the Galvanic cell measurements that electrons, and not oxygen ions or positively charged vacancies, are the major conduction current carriers in a n-type $BaTiO_3$-based ceramic of X7R specifications[40]. The increasing leakage current in degradation is enhanced by oxygen migration, as expressed by the equation[5,7]

$$O^{=} \longrightarrow \frac{1}{2} O_2 \uparrow + V_O'' + 2\ e'$$

where an oxygen vacancy V_O" and two conduction electrons are created for every oxygen ion $O^=$ generated by the application of voltage bias and/or by the elevated temperature of the ceramic.

Two models, using the concept of oxygen vacancy migration, have been developed to explain the exponential increase of leakage current with time[1,7,15]. The first model is based on the assumptions that the current is proportional to the conduction electron density and the conduction electrons are due to oxygen vacancies. Also, it is assumed that there is no supply of oxygen to replenish that which left. This model deals with oxygen vacancy migration, where oxygen vacancies migrate to the cathodes and the leakage current is enhanced by the conduction electrons that are generated at the anodes. This neglects the fact that the electron mobility is also changing with time.

The second model is based on the grain boundary phenomenon where the reduction of the grain boundary barrier height with time causes increase in leakage current. The same type of model has been used for poly-Si[51], ZnO varistor[52] and other semiconductor materials[20]. This model suggests that oxygen vacancies migrate to the cathode, while majority accumulate to the negatively charged grain boundaries of the n-type materials. In $BaTiO_3$-based ceramics, oxygen vacancies can accumulate at grain

boundaries and neutralize trapped electrons, resulting in reduced barrier height and consequent increase in leakage current. In applying such a model to high-K, high resistance materials that are often inhomogeneous, four basic assumptions are made:

(i) Grains and grain boundaries are homogeneous and uniform.

(ii) Charge due to the polarization discontinuity between grains is neglected.

(iii) The grain boundary potential barrier is due to the trapped electrons and the associated positive space charge.

(iv) The grain boundary itself is infinitesimally thin, with no second phase or other material present (with the possible exception of excess oxygen and dopant atoms).

Thus even though these assumptions are to varying degrees untrue (especially the first two), some conclusions can still be obtained for high-K, high resistance ceramic.

In addition, preliminary results indicate that the degradation is dependent compositionally upon both the Ba/Ti ratio and the dopant content[54]. Besides, it is known that ceramics exhibiting non-Ohmic current-voltage behavior are those that are most likely to degrade because of the current injection mechanism.

3.3 Grain Boundary Barrier and Grain Size

Grain boundary barriers play a predominant role in the electrical conduction processes in poly-Si materials[55,56], barrier layer capacitors[57,58], PTC(positive temperature coefficient) ceramics[29,59] and in varistors[61-63]. The grain boundary potential barrier is formed when the charges due to the electrons, holes or ionized impurities segregate and are trapped at a grain boundary, while an equal and opposite space charge is induced in the adjacent layer of the material.

The potential barrier, as illustrated for n-type homogeneous material in Fig.2(a) causes impedance to current flow in the form of a resistance R, where

$$R \propto \exp(\phi_B/kT) \quad \text{---------- (3.5)}$$

This grain boundary barrier height ϕ_B for homogeneous grain at zero bias can be expressed by[64]

$$\phi_{B(V=0)} = \phi_{BO} = \frac{q^2 N_{GB}^2}{8 \varepsilon N_i} \quad \text{----(3.6)}$$

where N_i = impurity (donor or acceptor) density in the grain (assumed completely ionized),

N_{GB} = state density of trap,

ε = permittivity,

q = electron charge.

A Reduction of ϕ_B can cause increase in leakage current in the material. For n-type semiconducting $BaTiO_3$ ceramics, it is known that one mechanism for the grain boundary charge is electrons trapped at oxygen species that are absorbed at the grain boundaries[65]. Also there exist several other possible types of grain boundary potential energy diagrams[10,66]. These include the following:

1) A normal polarization discontinuity at the grain boundary in homogeneous grains;
2) No charge at or near the grain boundary in homogeneous grains;
3) High resistance layer near the grain boundary in nonhomogeneous grains, shown in Fig.2(b);
4) Low resistance layer near the grain boundary in nonhomogeneous grains, indicated in Fig.2(c);
5) The presence of a second material or phase near the grain boundary in nonhomogeneous grains, illustrated in Fig.2(d).

A very important aspect of doped polycrystalline $BaTiO_3$ is the inhomogeneous distribution of the dopants. Studies

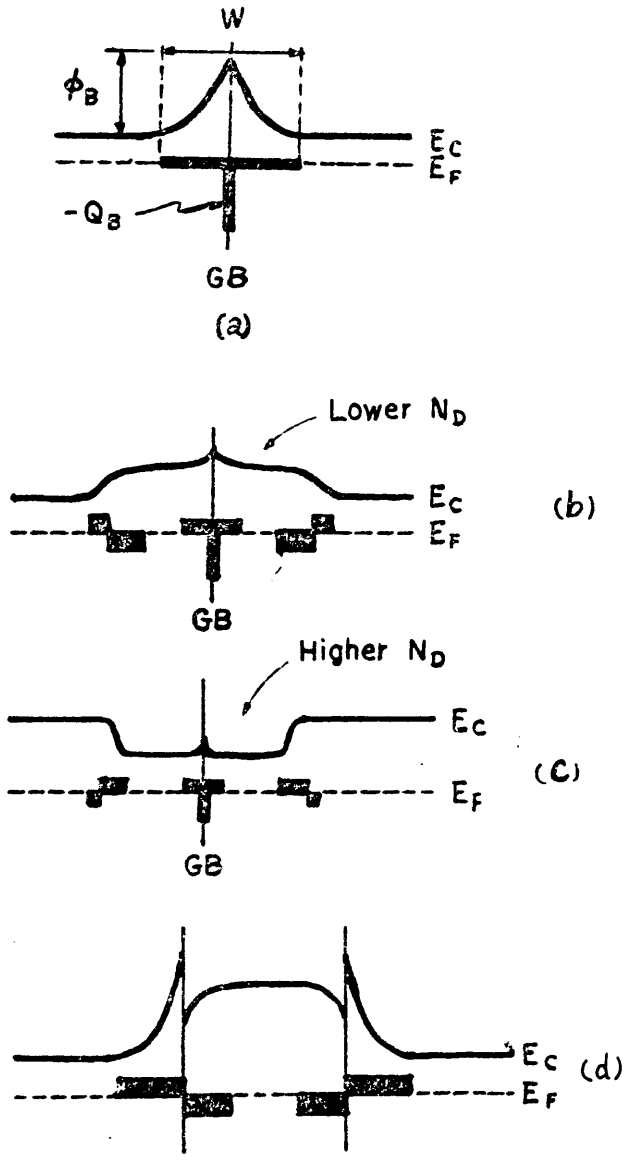

Figure 2. The energy diagrams for grain boundary potential barrier. [taken from (10)]

(a) Negative charge trapped at GB in homogeneous grains;

(b) High resistance layer near GB in inhomogeneous grains;

(c) Low resistance layer near GB in inhomogeneous grains;

(d) Presence of a thin layer of second material or phase.

have shown that a large fraction of the additives to $BaTiO_3$ are concentrated at the grain boundaries[13,67]. So the GB barrier height ϕ_B is determined by the donor density N_i and the grain size r_o for a given dielectric constant and the density of GB state density of the material. For large grains where the width of space charge W is smaller than the radius r_o of the grain, the grain is defined as being partially depleted. The barrier height is dependent on W and is given by[12]

$$\phi_B = \frac{q\, N_D\, W^2}{2\, K\, \varepsilon_o} \qquad \text{------ (3.7)}$$

where K and N_D are the dielectric constant and donor density respectively. For small grain size ($W > r_o$), reduction of the barrier height is due to the grains being totally depleted of mobile charges.

The total depletion of a grain will occur either if the donor density is low or if the grain size is small[7]. For a given grain size, the GB potential barrier will decrease if the donor densities are either less than or greater than the specific donor density N_{DO}. The specific donor density is defined by[12]

$$N_{DO} = \frac{N_{GB}}{2\ r_o} \qquad \text{--------- (3.8)}$$

For $\phi_{BO} \propto 1/N_D$ if $N_D > N_{DO}$,

and $\phi_{BO} \propto N_D$ if $N_D < N_{DO}$.

In addition, the grain boundary potential height is also affected by the grain curvature[19]. The barrier height decreases with decreasing grain size due to the increase in grain curvature. The grain shape, which is influenced by the grain curvature, has also an effect on the GB barrier height. It has been found through SEM, that the grain shape is cylindrical for NPO, nearly spherical for X7R and polygonal for Z5U ceramics[12].

It has been shown that for the same composition, increased sintering time decreases the dielectric strength. This has a strong correlation with the increase in grain size[59]. In doped $BaTiO_3$, it has been found that the large sized grains were semiconducting, having a conductivity much larger that the small sized grains[68].

3.4 Changes in Field Distribution with Time

The electric field applied to a single or polycrystalline $BaTiO_3$ may cause slow changes with time in current, potential distribution, or coloration. This phenomenon, though very interesting, is somewhat complex.

Goto and Kachi[46] used Kerr effect to optically study changes in the field distribution with time for $BaTiO_3$ single crystals with a minimum thickness of 0.42 mm. Lehovec and Shirn[45] used a movable probe and an electrostatic voltmeter to measure the voltage distribution across a 0.5cm thick $BaTiO_3$ ceramic as a function of time. Fig.3(a) illustrates the striking changes of field distribution with time for a single crystal. Fig.3(b) shows that the net space charge distribution changes with time. As can be seen in the figure, the field strength at anode at first increases and is then gradually decreased. But the field near the cathode is lower than the other position. Beyond stage (d), the field distribution appears to settle down to equilibrium state.In such a situation the field distribution inside the dielectric is more homogeneous and the field strength in the anode side region becomes almost constant. It has been found that the current is space-charge-limited at the initial stages of conduction. This process, taking place at the cathode, should be governed by the injection of electrons into the dielectric. Accordingly, there would be a pile up of an excess negative space charge, leading to a space-charge-limited current transport. It was proposed[45] that in polycrystalline $BaTiO_3$ samples, a high conduction region, found near the cathode is associated with the presence of trapped electrons in oxygen vacancies. It was assumed that

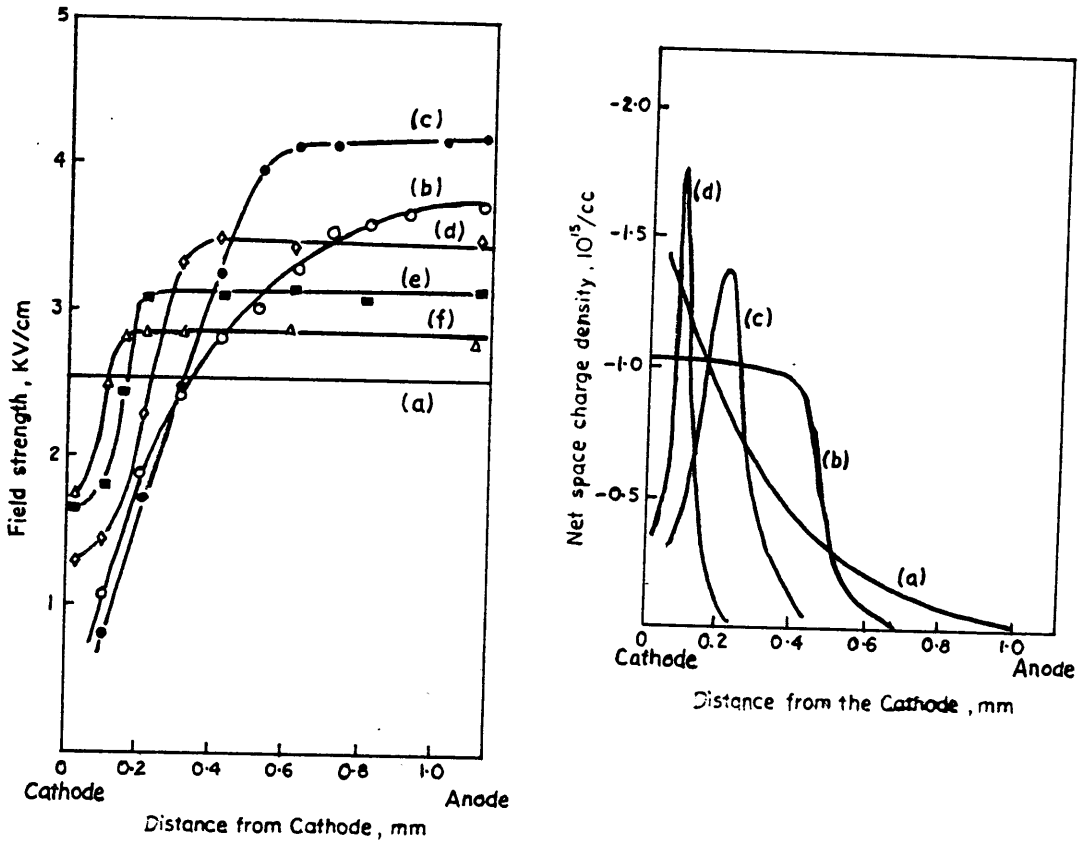

Figure 3. (i) Field strength as a function of the distance from the cathode at various times

(a) 10sec (b) 1.5hr (c) 7.5hr (d) 10hr (e) 18hr (f) 24hr

(ii) Net space charge distribution at various times

(a) 1.5hr (b) 7.5hr (c) 10hr (d) 24hr

[both taken from (46)].

the oxygen vacancies can be generated or annihilated at the anode and/or the cathode interface and at grain boundaries of the polycrystalline $BaTiO_3$. Some of the accumulated vacancies at the cathode would trap injected electrons. As a result, the conductivity at the cathode would increase with time.

In the succeeding stage the motion of the migrating oxygen ions (vacancies) would be responsible for the observed behavior in the equilibrium state. This does not always mean that the conduction is purely ionic. The conduction is influenced or enhanced by the migration of the ionic species even when the effective carriers are electrons or holes.

The analysis of the field distribution indicates the injection of electrons from the cathode followed by the migration of the oxygen ions in the material. However, in dealing with two types of mobile charges (electrons and oxygen vacancies), injection and extraction efficiencies should play a role of equal importance as the corresponding roles of electrons and holes in a bipolar semiconductor device. The critical dependence of injection efficiencies on the type of electrode, the electrode preparation and its mode of operation are all well appreciated.

One phenomenological result of electrical degradation is the appearance of a color change of the dielectric in certain cases[44,45]. It has been proposed that sample

darkening occurs due to oxygen depletion, where the darkening is due to the F centers (electrons trapped at oxygen vacancies[5,45]).

3.5 Effect of Temperature and Voltage Stress on Degradation

The degradation of insulation resistance of high-K, high resistance MLC capacitors is the primary failure mode of such devices. The degradation rate, being determined by the microstructure of the material, is usually characterized as a function of voltage and temperature. Apart from the degradation mechanism, empirical studies have shown that the lifetime (or mean time to failure) τ , under temperature-voltage stress, is inversely proportional to the exponential of the temperature and to the nth power of the applied voltage[16,17]. The factor n depends on the capacitor composition. The relative lifetime has been described in accordance with the empirical equation

$$\frac{\tau_1}{\tau_2} = \left(\frac{V_2}{V_1} \right)^n \exp\left[\frac{E_A}{k} \left(\frac{1}{T_1} - \frac{1}{T_2} \right) \right] \quad ---(3.8)$$

where E_A is the activation energy, τ_1 and τ_2 are lifetimes at voltages V_1, V_2, and temperatures T_1, T_2, respectively. This result has been shown valid for both DC an AC applications[16,70]. Two models have been developed to

explain that why capacitor lifetimes follow the equation(3.8). In summary, the mechanisms of degradation that were considered are i) oxygen vacancy generation which causes increase in carrier concentration, and ii) reduction of GB barrier height[1,7,15].

An approximate voltage dependence of the lifetime is calculated based on that the local effective fields are higher than the average applied field at submicroscopic sites such as at "detrimental" ions, or at microscopic sites such as at the grain boundary surface layers. This would be of the form $e^{\alpha V}$ for the field enhanced diffusion, where α is a constant, or V^n for electrostriction. Calculations show that the actual stress dependence of the field has n values between 1.1 and 1.9, with n = 2 being the maximum[16]. So the degradation rate is proportional to a function of voltage, either in the form of $e^{\alpha V}$ or V^n.

There is a gradual change in the type of failure mode that should be noticed. As voltage stress is increased, a larger percentage of capacitors fail in the avalanche breakdown (ABD) mode. This indicates failure owing to the presence of extrinsic defects. Intrinsic failure is characterized by a thermal runaway (TRA)[27]. Whether a capacitor has failed intrinsically or extrinsically may be determined by its leakage current versus degradation time relationship, as shown in Fig.4.

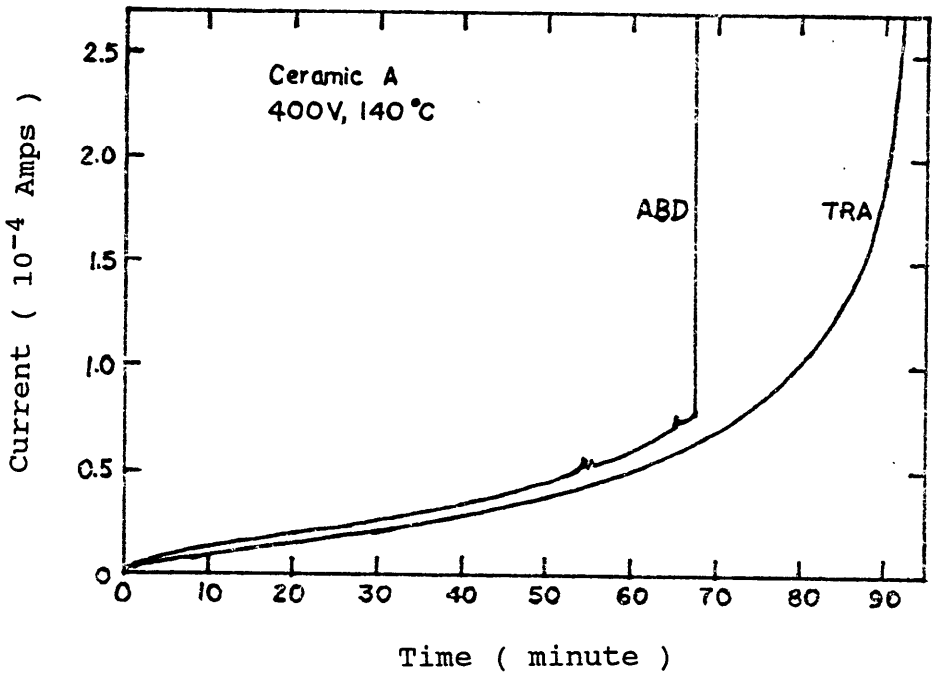

Figure 4. Leakage current as a function of time under high temperature and high voltage stresses. [taken from (27)]

Chapter 4: THEORETICAL BACKGROUND OF ELECTRICAL CONDUCTION

In $BaTiO_3$-based multilayer ceramic capacitors the electrical conduction is attributed to certain charge carriers and their modes of transport. This chapter presents the theoretical background for conduction mechanisms, which are necessary to interpret the results obtained from this research. The different types of leakage current due to different conduction mechanisms in an MLC capacitor are reviewed. Some of the proposed conduction mechanisms may be more pertinent to high-K, high resistance MLC capacitors than to other types.

4.1 Polarization Current

Polarization currents have been observed in a wide variety of dielectric materials, including a host of organic and inorganic "amorphous" solids[4]. The polarization currents were shown to dominate the low temperature-voltage response of dielectrics. Under such a low stress, the observed current consists of polarization current (which shows current value decreasing with time) and steady-state DC conduction current. There are a variety of mechanisms which give rise to polarization current, all of which may be present in a highly disordered layers or at the interface

thereto[2]. These may be associated with dipole movement or with the motion of charge carriers such as ions or hopping electrons[8]. This polarization current arises from the tendency of the polarizing species in the material to respond in a delayed manner to the exciting field.

Under DC applied voltage, the polarization current $I_c(t)$ follows a universal law as

$$I_c(t) = \frac{dP(t)}{dt} \propto t^{-m} \qquad \text{----(4.1)}$$

where a typical value of the exponent m lies below 1.0.

It would appear that the mechanisms of steady-state conduction and the origins of polarization currents are not directly related. They show a vastly different dependence on temperature and a large change in one do not evoke a similar change in the other[2].

4.2 Ohmic Current

Ohmic current is proportional to voltage and can consist of contributions from electronic (electrons and/or holes) and ionic carriers (cations, anions, and vacancies). The voltage dependence of the current is expressed as[6]

$$I = \frac{AV}{L} \sum_i q_i \mu_i n_i \qquad \text{-------- (4.2)}$$

where q_i is the charge of carrier i (Coulomb), A is the cross-sectional area (cm^2), L is the thickness (cm), n_i denotes the concentration of carrier type i (cm^{-3}), and μ_i is the drift mobility of carrier type i (cm^2/V sec.).

For transport dominated by hopping or by grain boundary transmission, the dependence of Ohmic current I is contained in n and μ, and may be expressed in terms of an activation energy E_A:

$$I = I_o \exp \left[- \frac{E_A}{kT} \right] \quad \text{------} \quad (4.3)$$

where I_o is a constant at a given voltage, and E_A is the sum of the carrier concentration and mobility activation energies, i.e. $E_A = E_{A,n} + E_{A,\mu}$.

4.3 Space Charge Limited Current (SCLC)

Space charge limited current occurs when the injected electrons (or holes) from the electrodes exceeds the native bulk carrier concentration. This current applies to electronic carriers because ions are not expected to be injected from the electrodes in MLC capacitors. A current-voltage relation for current emissions from a planar electrode is[71]

$$I = \frac{9}{8} A \theta \varepsilon \mu V^2 / L^3 \quad \text{------} \quad (4.4)$$

where ε is the permittivity and θ is a trapping parameter defined by

$$\theta = \left(\frac{N_c}{2\ N_t} \right) \exp \left[- \frac{\Delta E}{kT} \right]$$

where N_c is the conduction band density of states, N_t is the shallow trap density, located at energy $\Delta E (= E_c - E_t)$ where E_t is the energy of the trap centers.

Space charge limited current can also be emitted from a hemispherical point electrode to an anode or cathode because the electrode could not be perfect planar. The I-V relation for this type of SCLC is described by[72]

$$I = \frac{(2\ \pi\ )^{3/2}}{3} \mu (\theta q \varepsilon n)^{1/2}\ V^{3/2} \quad \text{---- (4.5)}$$

The two types of SCLC described above are due to electrode geometries and a single discrete shallow trap. In real cases, it is more likely that the I-V characteristics are modified towards a voltage exponent greater than two due to the distribution of trap energy levels[71,72], or spatially distributed shallow traps in the carrier density dependent mobility regime[74,75].

4.4 Schottky Current and Poole-Frenkel Current

Schottky or Poole-Frenkel current is caused by the

increase mobility of electrons or holes due to the lowering of the potential barrier by an external voltage. The Schottky effect dominates at the electrodes, while the Poole-Frenkel effect occurs at traps or grain boundaries in the bulk. Both currents have an exponential dependence on the electric field strength and can be expressed by the equation[6,72]

$$I = I_o \exp \left[\frac{B}{T} \left(\frac{E}{K} \right)^{1/2} \right] \quad \text{------} \quad (4.6)$$

where B is a constant, E is the electric field and K is the dielectric constant.

The Schottky effect only occurs at a rectifying contact, and probably does not apply to MLC capacitors. The Poole-Frenkel effect is more likely to be due to the possibility of electrons located in potential wells at the traps and at the grain boundaries.

4.5 Small Polaron Hopping Mechanisms

Two possible types of electronic conduction mechanisms exists that are pertinent to some polycrystalline oxides. One is the grain boundary barrier transmission which is based on band conduction. The other is hopping transport. It is expected that the charge carrier drift mobility for the

former is much larger than that for the latter.

A narrow conduction band and strong interaction between electronic carriers and lattice-phonons results in the formation of a polaron (a quasi-particle, i.e. the electron plus the associated strain field). The size of polaron is smaller than the interatomic spacing. Owing to the lattice translational symmetry, in such a system a localized state is quasi-stationary and occurs only at sufficiently high temperatures where the time between the consecutive hops is shorter than the decay time of a small-polaron wave packet located at a site[76].

This polaron effect occurs mostly in ionic crystal because of the strong Coulomb interaction between ions and electrons. In covalent crystals, the effect is weak because the neutral atoms have only a weak interaction with electrons. Also, in disordered systems, because of the lack of long-range order, stationary localized one particle states may exist, the amplitude of which decreases with increasing distance from the localization center. However, due to the interaction with lattice phonons, however, hopping transitions may occur among the localized states.

The strength of the electron-lattice phonon interaction is measured by the dimensionless coupling constant α given by[77]

$$\frac{1}{2}\alpha = \frac{\text{Deformation Energy}}{\hbar\omega_L} \quad \text{----- (4.7)}$$

where ω_L is the longitudinal optical phonon frequency near zero wavevector.

In polaron hopping transport, the electron associated with a large polaron moves in band. The effective band mass is increased by the deformation of the lattice. The electron associated with a small polaron spends most of its time trapped in a single ion.

For small polaron hopping, at high temperatures, the small polaron moves from site to site by thermally activated hopping. At sufficiently low temperatures, the small polaron becomes band-like with a large polaron effective mass m^*_{pol} given by

$$m^*_{pol} = m^* \left(\frac{1 - 0.0008\alpha^2}{1 - \frac{1}{6}\alpha + 0.00034\alpha^2} \right) \quad \text{----- (4.8)}$$

where m^* is the effective band mass, and α is the coupling constant given by Eqn.(4.7). In very low temperature range, this band transport and the (under barrier) hopping transport are due to the tunnelling process.

Small polaron hopping mobility μ_{pol} is expressed by[76]

$$\mu_{pol} = \mu_o \frac{1}{2\pi} \frac{\hbar\omega_o}{kT} \exp\left(- \frac{E_a}{kT} \right) \text{----(4.9)}$$

where ω_o is a characteristic phonon frequency, E_a is the height of the energy barrier the hopping carrier must overcome, μ_o is a constant, and the other symbols have their usual meanings. Consequently, for hopping transport, the drift mobility may be much less than 1 cm^2 / V sec.[76].

It is noted from eqn.(4.9) that the drift mobility is an exponential function of inverse temperature. This form of relationship is the main signature of small polaron hopping transport.

Chapter 5 : EXPERIMENTAL TECHNIQUES

5.1 Materials Used

Several different types of commercial ceramic capacitor samples were tested as a part of this research effort. The main focus, however, was on ferroelectric MLC capacitor samples having high dielectric constant.

Of the tests that were performed, capacitance versus time measurements were taken on the Corning 100 nF X7R and the Centralab 1 μF Z5U multilayer ceramic capacitors. Leakage current against time measurements were made on X7R MLC capacitors (Corning Electronics), Z5U MLC capacitors (Centralab Corp.), and PLZT MLC and NPO capacitors (Sprague Electronic Company). Degradation measurements were performed on using X7R MLC capacitors manufactured by Mouser Electronics, Z5U MLC capacitors manufactured by Centralab Corp.

No advance preparation of samples was necessary for the measurements. The as-manufactured multilayer ceramic capacitors were soldered directly into the setup used for these measurements. The measurement setup will be discussed in section 5.2, 5.3 and 5.4.

Several structural and electrical properties of the capacitor samples tested are listed in Table 1. A geometric structure of a multilayer ceramic capacitor chip is

illustrated in Fig.5.

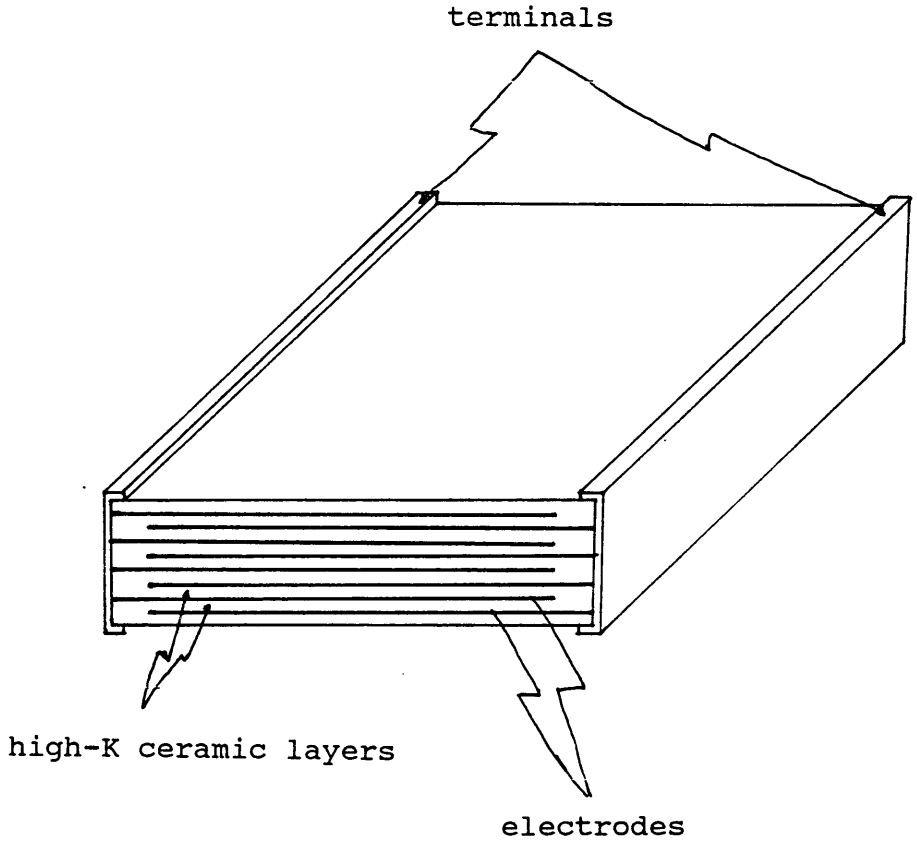

Fig.5 Structure of a multilayer ceramic capacitor

5.2 Low-stress Leakage Current Measurements

The setup for leakage current measurements was a simple series electric circuit consisting of a DC voltage power supply, a programable electrometer, a scanner with maximum

Table 1. A list of parameters of the samples

Type	Manuf.	K	number of layers	dielectric thickness	C	electrode material
X7R	Corning	2000	13	55 μm	100nF	Pb-based
	Mouser		19	20 μm	100nF	
Z5U	Centralab	5000	23	22 μm	1 F	P_d/A_g
PLZT	Sprague	1850	17	10 μm	78nF	P_b/S_n
				20 μm	39nF	
				30 μm	26nF	
NPO	Sprague	100	1	490 μm	56pF	

****

Type	Manufacturer	#A/d (cm)
X7R	Corning	$5.65*10^2$
Z5U	Centralab	$2.26*10^3$
NPO	Sprague	6.3

A is the area of electrode(cm^2), and d is the dielectric thickness(cm).

ten channels, and a maximum ten-sample adapter that was shielded and fixed in a temperature controlled furnace. A Hewlett Packard 6116A DC power supply was used to supply voltages from 0 to 100 volts. A Keithley 705 scanner was used to scan the ten samples sequentially. The leakage current was measured with a Keithley 617 programable electrometer. Ten 1MΩ resistors were hooked in series with the capacitor samples under test to protect the electrometer in case of device failure (shorting). These ten resistors also helped to lower the circuit noise level.

The MLC capacitors used for leakage current measurement were soldered into the circuit in the adapter. A Tenney Jr. temperature controlled oven was used to heat the samples. The furnace temperature could be set from -80 ^{o}Cto +200 ^{o}C with temperature variation less than $\pm$ 0.15 ^{o}C.

An IBM-XT personal computer was used to control the measurement system. A control program in Basic sets the measurement parameters, stores the data and processes the data into a graphic result.

Teflon high temperature coaxial cable is approperate for leakage current measurements because of its high resistance and low noise level at high temperatures.

A schematic of the experimental setup is shown in Fig.6.

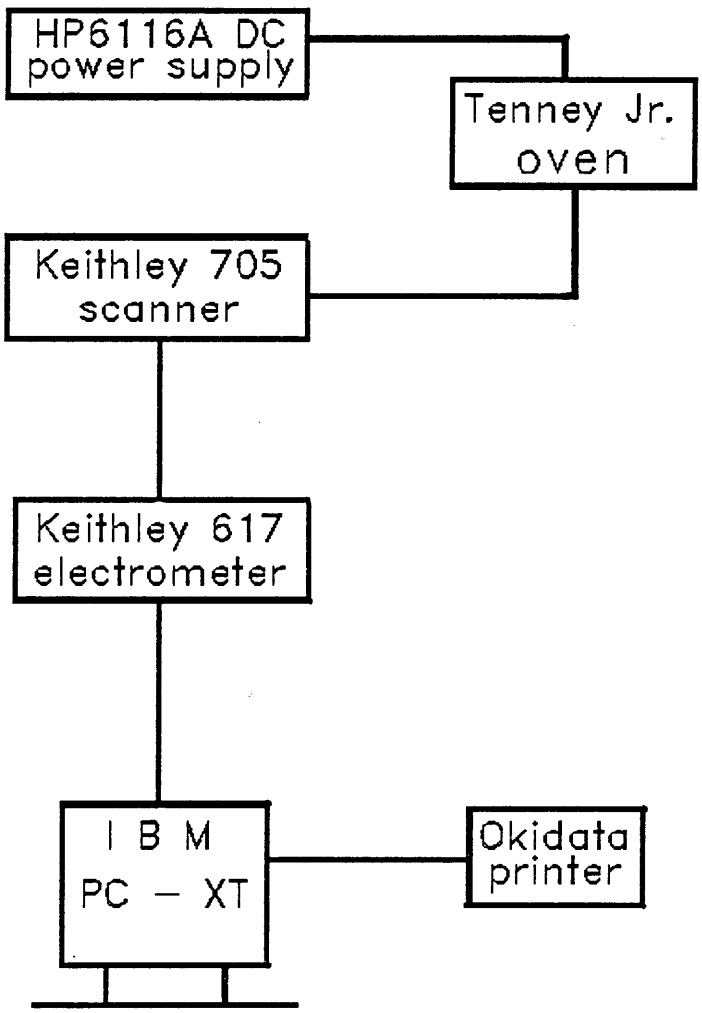

Figure 6. The leakage current measurement block diagram.

5.3 High-stre eakage Current (Degradation) Measurements

A test em, similar to that for leakage current measurements r low-stress condition, was used for the degradation surements. As high voltages and high temperatures required for MLC capacitors to degrade, a Hewlett Pack 515A DC power supply of the voltage range from 0 up to volts, and a Model 51894 Lindburg furnace having the m controlled temperature of 1100 °C were used for thipose.

Teflon temperature coaxial cable with a maximum operating teture of 295 °C was used in the setup. The MLC chip sa were soldered into the test circuit by means of ann Multicore high temperature solder (296 °C). The endhe Teflon cables at which the chip samples were solden, were kept stationary on a ceramic substrate usega non-conductive epoxy. This was done in order to rthe noise level that may be caused by mechanical ons. The chip samples were then heated in the furnace the set temperature. The measurements were recorded onctemperature was stabilized.

5.4 Time-dep e Measurements of Capacitance

The cap e of a MLC capacitor changes slowly with time under stress. The time dependence measurements

of capacitance were undertaken by using a Hewlett Packard 4192A Impedance Analyzer with an attachment allowing DC voltage bias up to + 200 volts. The frequency ranged from 5 Hz to 13 MHz. The capacitor temperature was maintained in the range of 25 ^{o}C to 125 ^{o}C. The capacitance was measured at definite time intervals, each measurement being recorded through the impedance analyzer in the parallel circuit mode.

Chapter 6: RESULTS AND DISCUSSION

A generic leakage current versus time relation in high dielectric, high resistance $BaTiO_3$-based ceramic has been reported[1]. Substantial amount of measurements were performed with MLC capacitors under different voltage-temperature stresses to present leakage current versus time characteristics in this research effort.

Fig.7 shows the leakage current versus time characteristics for a stressed dielectric, which generally follow a bathtub-shaped curve. The leakage current-time curve can be divided into three different regions corresponding to various contributions to the leakage current. Based on the experimental results, it is concluded that the leakage current in region 1 is predominated by polarization current, which is caused by dielectric polarization mechanisms. In region 2 the steady-state leakage current is produced by mobile charge carrier motion under applied voltage. The charge carriers that contribute to leakage current may be electrons, holes and ions (cations, anions, and vacancies) in ceramic. The leakage current in this region is defined as DC conduction current. In region 3 the leakage current increases with time, which is indicative of degradation phenomenon. Increasing leakage current deteriorates the properties of a device leading eventually to a complete failure.

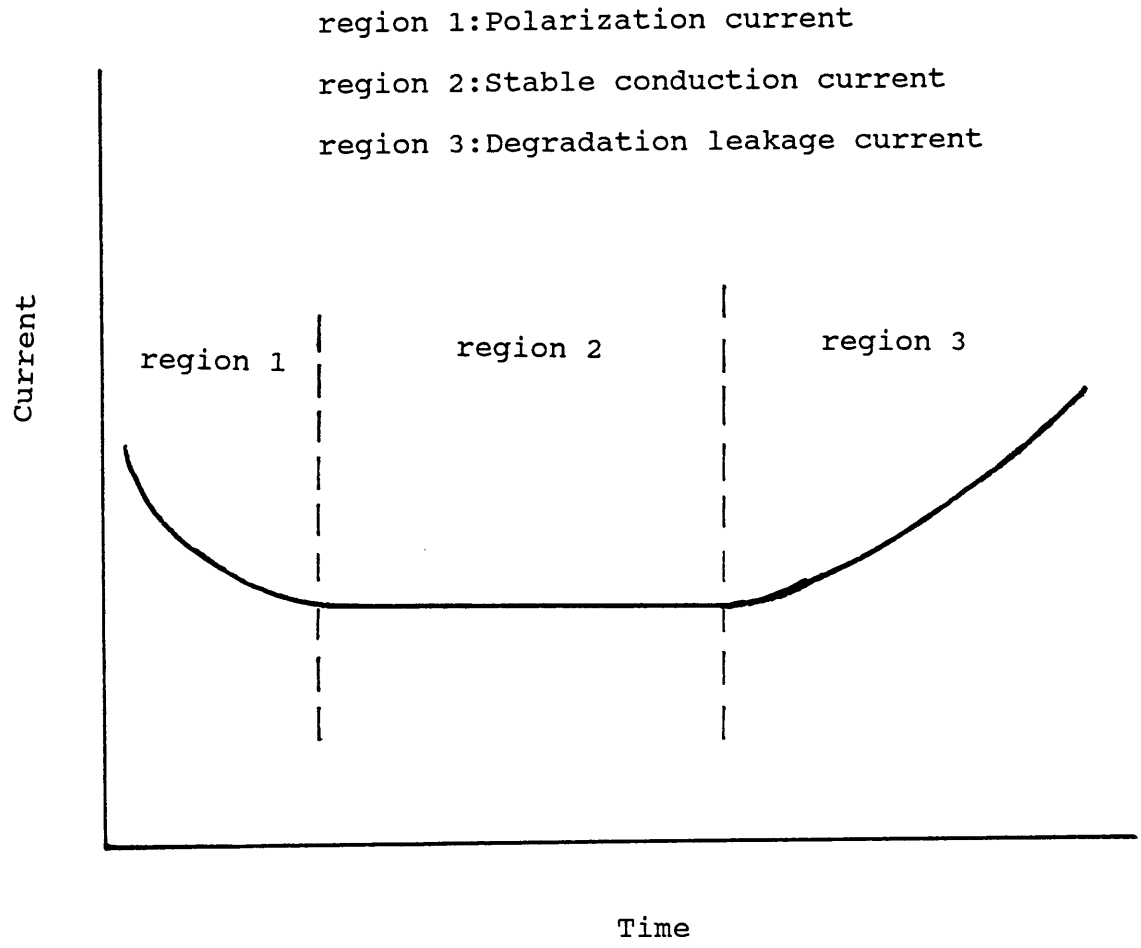

Figure 7. Leakage current versus time for a stressed dielectric generally follows a bathtub-shaped curve.

The leakage current behaviors and their corresponding mechanisms in three different regions will be discussed in detail in the following sections.

6.1 Polarization Current-Time Relationships

The current-time characteristics at low temperature and low voltage stress exhibit a current decay. In the low stress leakage current experiment, the measurement temperature is lower than or equal to the Curie temperature of the $BaTiO_3$-based ceramic while the maximum applied DC voltage is less than 100 volts.

According to the reported phenomenon[4], the observed leakage current decreases with time in a wide variety of dielectric materials. This includes a host of organic and inorganic "amorphous" solids[2,3,4] The leakage current-time measurements were performed on barium titanate based MLC capacitors. Based on the experimental results, a more detailed current-time relation was revealed. The observed leakage current-time characteristics for dielectric solids can be expressed in a power law relation as

$$I_L(t) = I_o\, t^{-m} \qquad \text{---------- (6.1)}$$

where exponent m is the power value and I_o is a constant for

a given voltage and temperature. This relation is shown in Fig.8 for I-t curves plotted on log-log scale for both X7R and Z5U MLC capacitors. The magnitude of the power value m in Eqn.(6.1) can be obtained by measuring the slope of the I-t curve. It was found that the power value m is determined by the microstructure of the dielectric material. The m value is strongly dependent on temperature and is slightly dependent on applied DC voltage.

The leakage current $I_L(t)$ in a MLC capacitor under low temperature and low voltage stress essentially consists of conduction current (resistive current) $I_R(t)$ which is generally a stabilized current value under low stress, i.e. $I_R(t) \approx I_R$, and polarization current (capacitive current) $I_C(t)$. The leakage current can be expressed as

$$I_L(t) = I_C(t) + I_R \quad \text{--------- (6.2)}$$

From the experimental results of the $BaTiO_3$-based MLC capacitors, it is known that the leakage current $I_L(t)$ under low constant stress is predominated by polarization current $I_C(t)$ which obeys a power law $I_C(t) = I_o\ t^{-m}$. After a sufficient long time (hours or days at room temperature), the leakage current reaches a steady-state value, i.e. conduction current representing a true electronic current flow in the test circuit as opposed to polarization

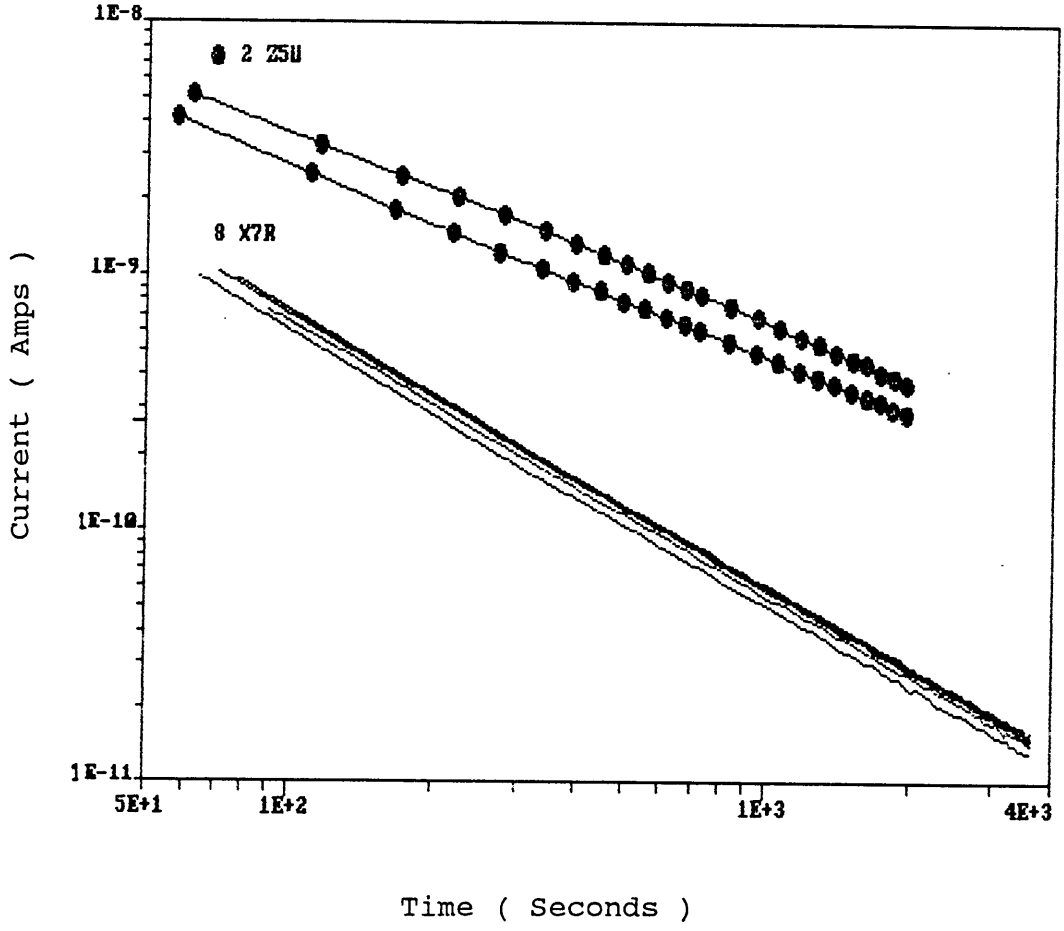

Figure 8. Leakage current-time characteristics of eight X7R and two Z5U devices at T = 25 ^{o}C and V = 50 volts.

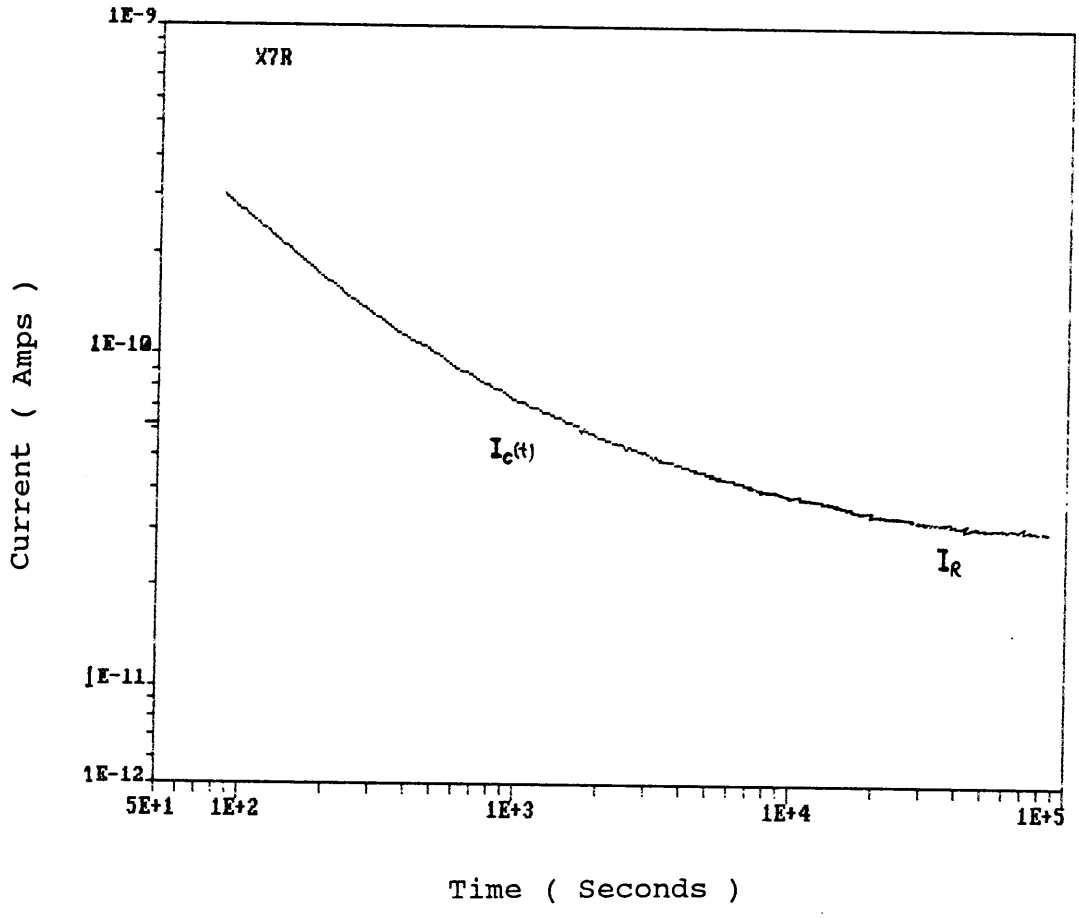

Figure 9. Leakage current stabilization behavior of X7R at T = 100 ^{o}C and V = 20 volts.

current which corresponds to a localized charge displacement in the materials. This procedure can be accelerated by increasing ambient temperature as shown in Fig.9.

The significances of Eqn.(6.2) will be discussed in the following two subsections according to the two terms which indicate two different mechanisms of leakage current flow.

6.1.1 DC Conduction Current Contribution

The second term I_R in Eqn.(6.2) indicates a DC conduction current contribution to the total leakage current in a MLC capacitor. Considering that Ohmic current is the predominant contributor to the DC conduction current (as is usually true for $BaTiO_3$-based MLC capacitors because SCLC, Schottky and Pool-Frenkel current contributions may be negligible under low voltage stress), the conduction current possibly can consist of electronic(electrons and/or holes) and ionic contributors. It has been found that electronic current is dominant in $BaTiO_3$-based ceramics at the temperature below 500^oC[35,36,40]. The electrical transport is mainly due to hopping or grain boundary transmission. It is the possible charge carrier transport mechanisms in X7R and Z5U MLC capacitors. Therefore, the DC conduction current I_R is expressed as a function of voltage and temperature[6] as follow

$$I_R(V,T) = \frac{qAn\mu V}{L} \exp[-\frac{E_A}{kT}]$$

where q --- electronic charge;

A, L --- cross-section area and thickness;

n --- electron or hole concentration;

μ --- charge carrier drift mobility.

$E_A = E_{A,n} + E_{A,\mu}$ is the sum of the concentration activation energy and mobility activation energy. For certain type of X7R MLC capacitor, the conduction current is thermally activated with an activation energy E_A = 1.3 eV while E_A = 1.26 eV for certain type of Z5U MLC capacitor.

DC conduction current I_R should be a steady-state current value. It was found from the experiment that the DC conduction current density in Z5U MLC capacitors is about six times higher than that in X7R MLC capacitors under the same test condition.

6.1.2 Polarization Current Contribution

The first term $I_C(t)$ in Eqn.(6.2) represents the polarization current portion in the total leakage current. The polarization current in dielectrics decreases with time following a power law $I_C(t) = I_o\ t^{-m}$. In dielectric materials the relaxation of localized charge(ions or electrons) displacement in an external electric field

results in this type of current-time relationship.

The charge displacement processes, according to a many-body interaction model[4], can be determined by three mechanisms as charge localized hopping(short-range hopping between neighbors)[8,9], configurational tunnelling transitions of the flip and flip-flop transitions. Macroscopically, these charge carrier displacement processes is expressed as dielectric displacement D(t) in dielectric materials. Thus

$$\vec{D}(t) = \varepsilon_o \vec{E}(t) + \vec{P}(t)$$

where ε_o is permittivity in vacuum. $\vec{P}(t)$ is polarizability and $\vec{E}(t)$ denotes a spatially uniform electric field attributed to applied voltage. The dielectric displacement gives the total charge density current induced at the electrodes

$$I_C(t) = \frac{dD(t)}{dt} = \varepsilon_o \frac{dE(t)}{dt} + \frac{dP(t)}{dt}$$

Considering the DC applied voltage E(t)=0, only the change of the polarizability with time results in the polarization current. The relation of the polarization current with time can be expressed

$$I_C(t) = \frac{dP(t)}{dt} = I_o\, t^{-m} \quad \text{--------} \quad (6.3)$$

Compared with the activation energy of 1.3 eV for conduction current I_R in X7R, the polarization current $I_C(t)$, evaluated for a given time t in X7R can also be experimentally characterized by its pseudo-activation energy E_{Ap}. In the condition of T < 125 ^oC, the pseudo activation energy is 0.35 eV at time t = 100 second, and E_{Ap} = 0.57 eV at time t = 600 second after a DC voltage was applied. It was found from the experiment that the pseudo-activation energy for polarization current increased with time until it reached to the conduction activation energy value, i.e. E_A = 1.3 eV, for X7R. This process corresponds to the phenomenon that the polarization current predominates the initial stage of the leakage current, and then the DC conduction process gradually becomes more effective till the conduction current eventually predominates the leakage current. Such current transition behavior is depicted in Fig.9.

The leakage current versus time relation at different temperatures is shown in Fig.10. For X7R MLC capacitors,as the temperature increases, the electron long-range hopping conduction process is thermally activated. Thus the conduction currents become dominant in the total leakage

currents as the temperature increases.

The fact that polarization current decreases with time, as shown in Fig.8, was confirmed experimentally by discharge current measurement and by time-dependence of capacitance measurement.

(i) Discharge Current Measurement

Using the discharge current technique, we were able in this way to completely isolate the polarization current from the true equilibrium DC conduction current since the discharge current represents only the transient polarization effects, while the charge current contains the equilibrium DC component as well.

Fig.11 shows the characteristics of charge current and discharge current versus time for both X7R and Z5U obtained at room temperature and 50 volts. Both current-time relations obey the power law of the same exponent m value, as described as Eqn.(6.3). These experimental results indicate that, at initial stage after voltage is applied, the leakage current measured at room temperature and in low voltage range is actually the polarization current.

This indicates that the applied voltage values should lie in the Ohmic region of the current-voltage curve. If the voltage is higher than the threshold voltage obtained by current-voltage measurement, other current factors, such as SCLC, may be involved in the polarization current value

using discharge current measurement. Fig.12 shows the characteristics of charge and discharge currents versus time of X7R at 400 volts. It is noticeable in the graph that the discharge current level is higher than charge current level. There exists a crossover between the two currents.

The current crossover phenomena is completely incompatible with the response of a linear system, i.e., the difference between the charge and discharge currents should be equal to the time-independent conduction current. In this case the current crossover phenomenon could be explained as a space charge limited current effect[10]. Since the value of applied DC voltage was 400 volts, which exceeded the Ohmic region of I-V characteristics for X7R, the existing current crossover could be due to the injection of space charge into the dielectric during the charging process, leading to gradual accumulation of excess charge density near one or both electrodes, according to the nature of the interface. This phenomenon is also probably due to the trap-fill and trap-release process if there are shallow traps uniformly distributed inside the material (which could be distinguished by low-frequency measurement)[4].

Thus it can be concluded that the reasonable polarization current measurement can only be undertaken at the voltages within the Ohmic region of I-V characteristics.

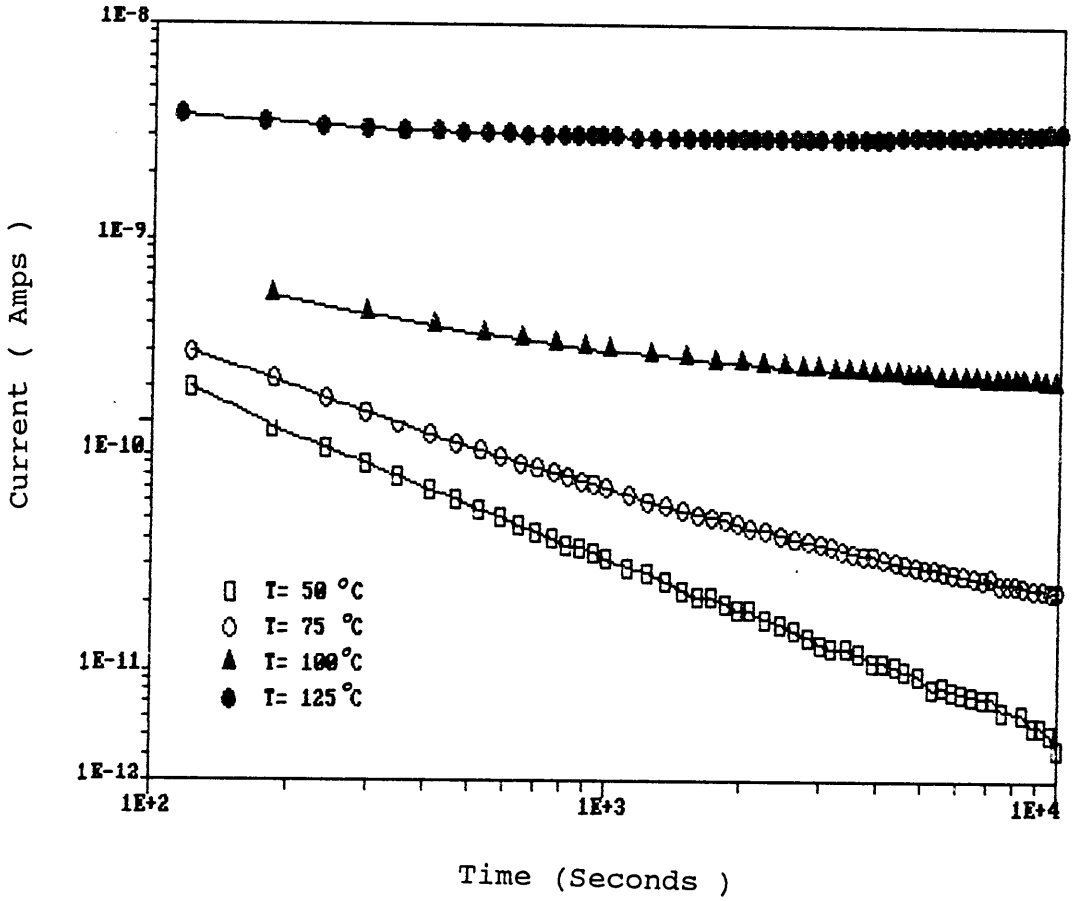

Figure 10. Leakage current-time characteristics for X7R capacitors at different temperatures, and at V = 100 volt stress.

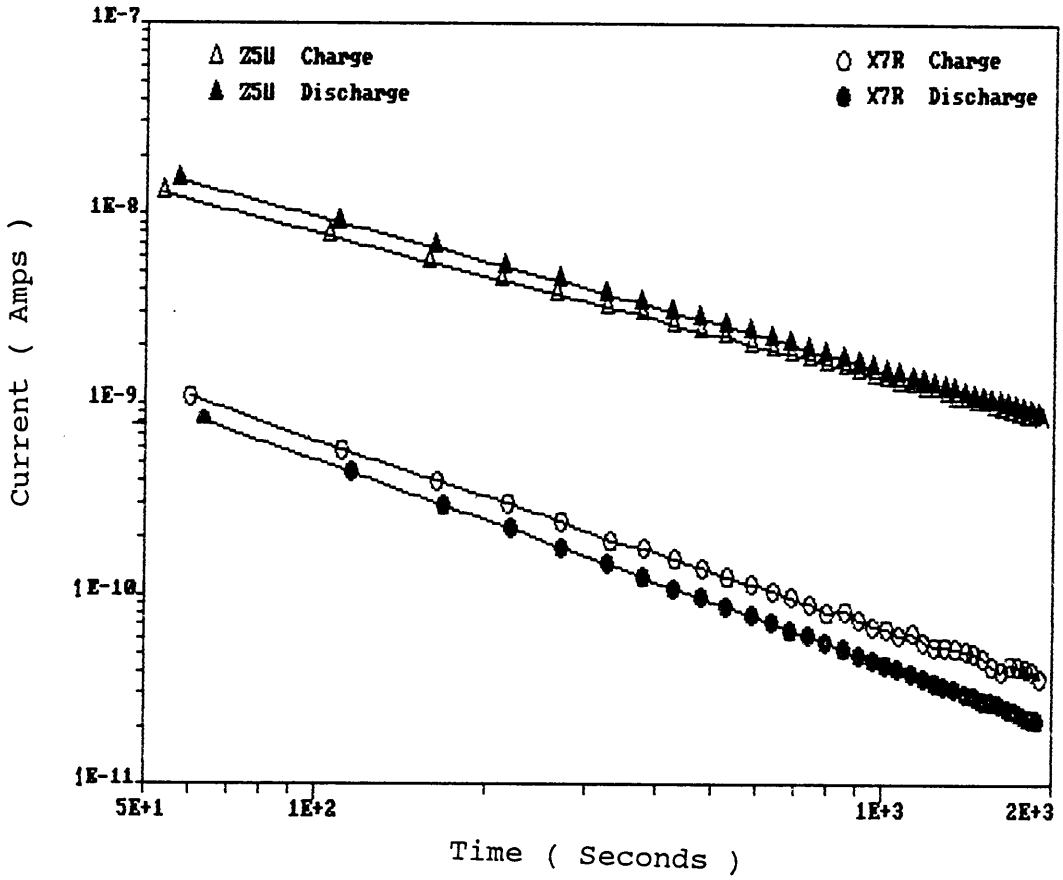

Figure 11. Charge currents and discharge currents decreasing with time in X7R and Z5U at T = 25 ^{o}C and V= 50v.

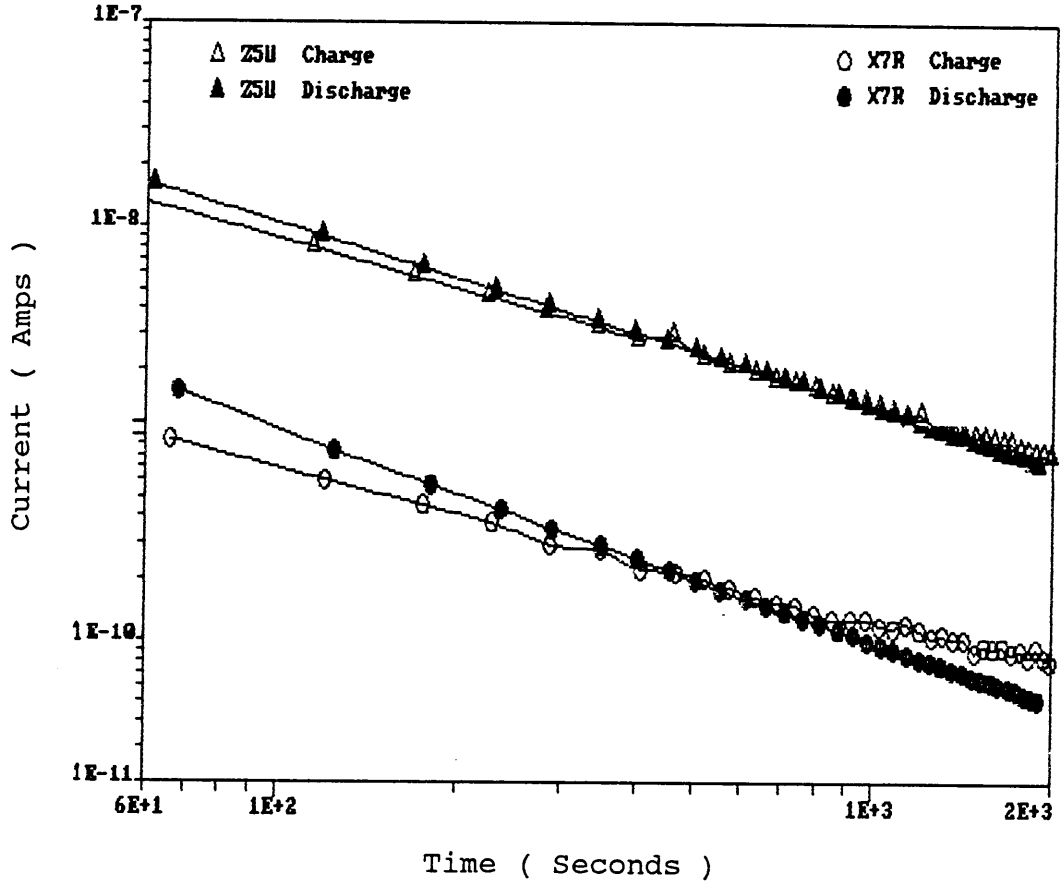

Figure 12. Charge currents and discharge currents versus time for X7R and Z5U at T = 25 ^{o}C and V = 400v.

(ii) Capacitance versus Time Measurements

Assuming that the power law given by Eqn.(6.3) is valid only at low temperature(about room temperature) in the entire physically accessible time range, we may write the following expressions for the polarization in the charging mode[4]

$$P(t) = \varepsilon_o E_o \int_o^{\infty} f(t)dt = \frac{A}{1 - m} t^{1-m} \quad \text{----- (6.4)}$$

for $0 < m < 1$, where ε_o is permittivity in vacuum, E_o is steady electric field, and $f(t) \propto t^{-m}$ is dielectric response function which characterize the response of the dielectric medium to specified electric excitations. A, in Eqn.(6.4) is a constant determined by material.

For $m = 1$, there exists a singular solution for which the polarization should show a logarithmic time dependence since

$$\int_a^t \frac{1}{t} dt = \ln t - \ln a \quad \text{----- (6.5)}$$

where a is a constant. It is interesting to investigate in more detail the transition from the power law (6.4.1) and (6.4.2) relations to the logarithmic law (6.5) as the

exponent m value approaches the critical value 1.

Therefore, the capacitance-time relation may be described as

$$C(t) \propto P(t) \propto b \ln t \quad \text{------} \quad (6.6)$$

where b is a constant much smaller than unity ($b << 1$). C(t) illustrates that capacitance is time dependent.

The exponent value m's for X7R and Z5U at room temperature are $m_{X7R} = 1$ and $m_{Z5U} = 0.85$, respectively. The discussion of exponent m will be given in the next subsection. The results of capacitance-time measurements show the following C-t relation

$$C(t) = C_o - C_1 \ln t \quad \text{------} \quad (6.7)$$

where C_o and C_1 are constants. The experimental expression (6.7) is exactly in the same form as the C-t relation theoretically described in Eqn.(6.5).

Fig.13 represents the C-t characteristics of X7R MLC capacitor at room temperature. The capacitance decreases with log time as expressed in Eqn.(6.7). The C_1 value can be obtained from the slope of C-log t curve, while the C_o value is measured from the intersection of the curve on vertical axis.

The polarization current could be obtained by

differentiating Eqn.(6.7)

$$I_C(t) = V\frac{dC(t)}{dt} = \frac{C_1 V}{t} \qquad \text{--------- (6.8)}$$

where V is the applied DC voltage.

Table 2 below gives a comparison of the calculated polarization current values using Eqn.(6.8) with the values measured in the same conditions for X7R and Z5U MLC capacitors.

Table 2: A comparison of polarization current values obtained in different ways

T = 25 ^{o}C

Sample	V (volt)	C_1 (Farad)	t (sec.)	$I_C=C_1V/t$ (amps)	I_L(measured) (amps)	I_C/I_L (%)
X7R	100	3×10^{-10}	100	3×10^{-10}	3×10^{-10}	100
			500	6×10^{-11}	5.6×10^{-11}	107
			1000	3×10^{-11}	2.8×10^{-11}	107
			2000	1.5×10^{-11}	1.4×10^{-11}	107
Z5U	10	2.84×10^{-8}	100	2.84×10^{-9}	2.9×10^{-9}	97
			500	5.68×10^{-10}	7×10^{-10}	81
			1000	2.84×10^{-10}	3×10^{-10}	94
			2000	1.42×10^{-10}	1.6×10^{-10}	88

It is evident, as shown in the table, that the calculated polarization current values using Eqn.(6.8) are very close to the measured leakage current values. The constant error ($I_C(t)/I_L(t)$ X 100% = 107%) for X7R was probably due to using different individual devices for I_L-t and C-t measurements.

From the calculated and measured I_C values for Z5U, the error value ($I_C(t)/I_L(t)$ X 100%) is variable. The error is generally greater than those for X7R. It is probably due to the fact that the exponent m value of Z5U is smaller than unity. The small m value(smaller than unity) may cause some errors in approximately using Eqn.(6.7) and (6.8) because the condition for relation (6.5) to be valid is not fully satisfied.

As a result, Fig.14 shows that the capacitance decrease results in initial leakage current that decreases roughly inversely with time, and increases linearly with applied voltage.

6.1.3 Effect of the Exponent m

Leakage current versus time measurements for ferroelectric ceramic capacitors (X7R and Z5U) and dielectric ceramic NPO capacitor (nonferroelectric) were performed under low temperature and low voltage stresses.

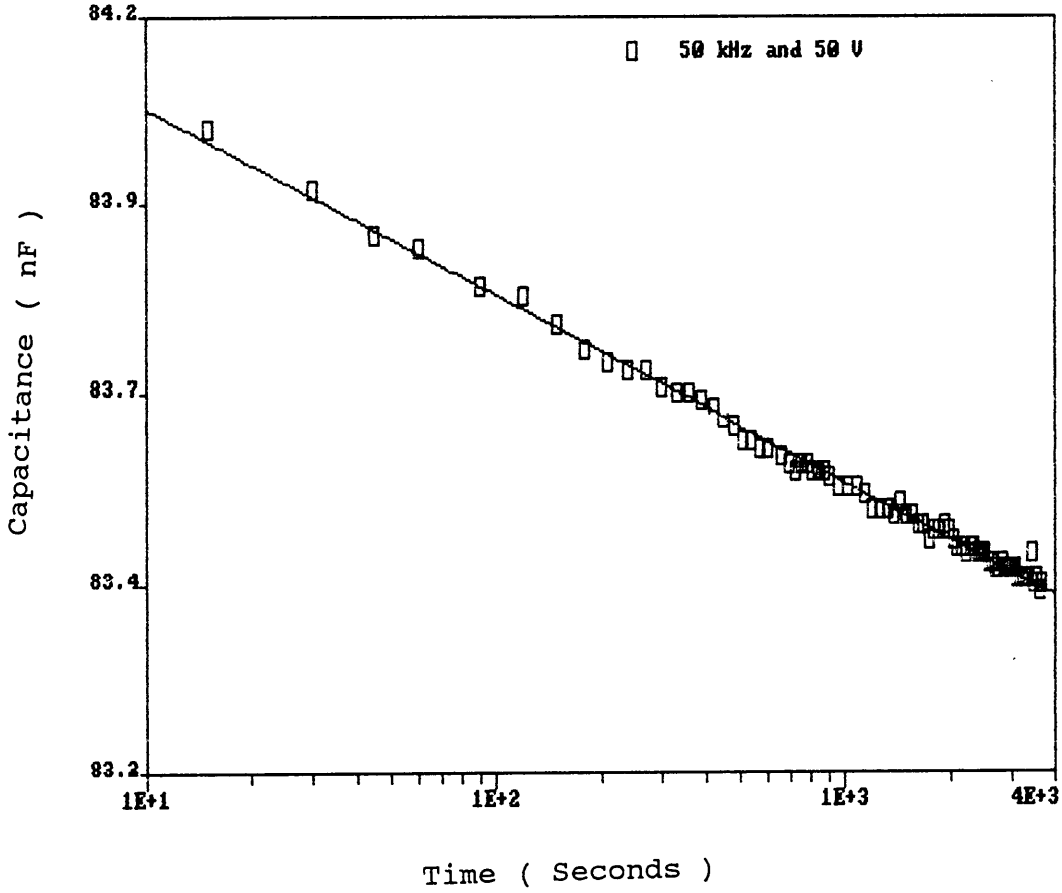

Figure 13. Capacitance-time characteristic for X7R under 50 volts bias, at room temperature and at f = 25kHz.

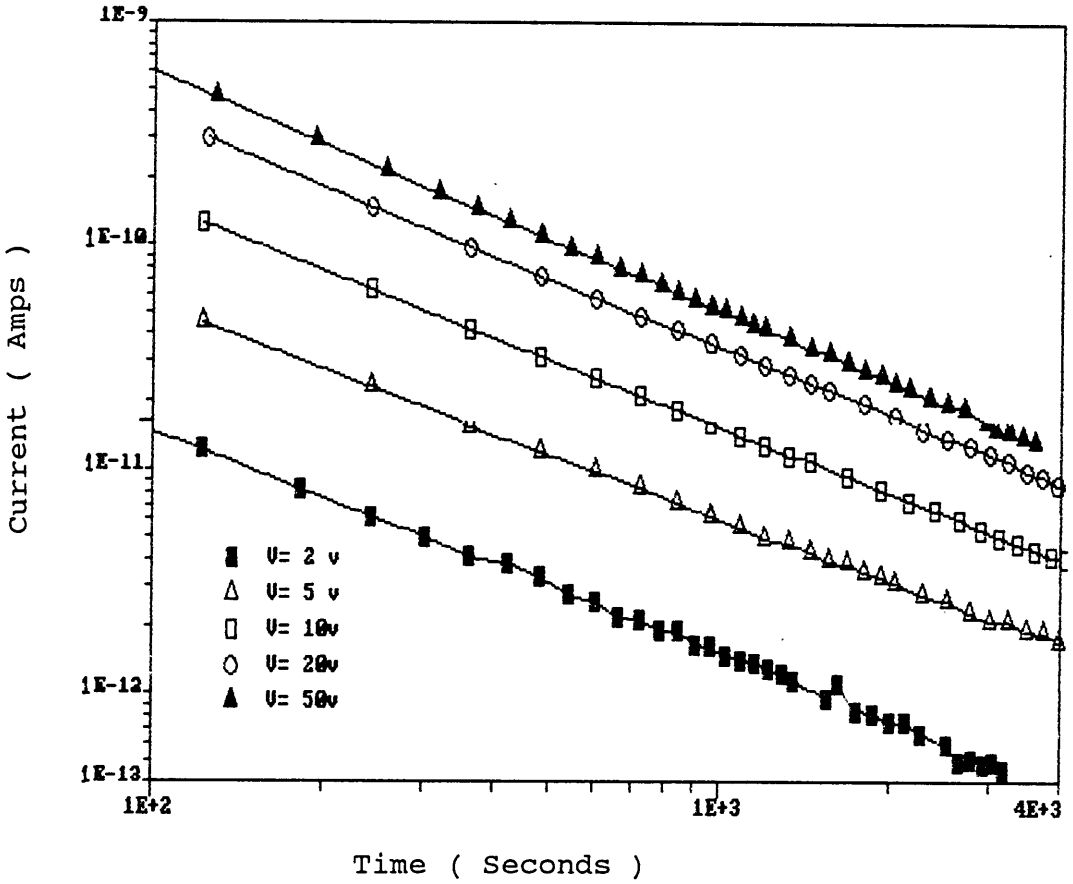

Figure 14. Leakage current-time characteristics for X7R due to capacitance decreasing with time, at T = 25 ^{o}C.

It has been established, based on the experiment, that the initial current of the leakage current is predominated by the polarization current. The I-t characteristics follow a power law

$$I_L(t) = I_C(t) = I_o\, t^{-m} \quad \text{----- (6.9)}$$

The magnitude of the exponent m is determined by several factors. To understand the behavior of m, the following two questions need to be answered:

* what does the m value tell us about the properties of the capacitor tested?

* what parameters affect the m value?

As we know, dielectric relaxation could cause frequency-dependence of capacitance and of dielectric loss. According to dielectric relaxation theory[4], the capacitance and dielectric loss would be less frequency-dependent as the exponent m value approaches 1. The m value lies in the range $0 < m \leqslant 1$. As the m value decreases, the dielectric constant and the dielectric loss become stronger dispersion with frequency.

Fig.15 shows the capacitance versus frequency characteristics for both X7R and Z5U MLC capacitors at room

temperature. Also the dissipation factor (D) versus frequency relations of X7R and Z5U under 10 volt bias are illustrated in Fig.16. It is evident that the capacitance value and dissipation factor of Z5U are more frequency-dependent than X7R. These characteristics arise from the m value, which for Z5U is less than the m value for X7R. According to the results of leakage current measurements at room temperature, m value equals to 1 for X7R while the m value is about 0.8 for Z5U.

In order to know the factors which may affect the m value, different types of ceramic capacitors were used in I-t measurements. The three types of capacitors are X7R, Z5U and NPO MLC capacitors. The I-t measurements were performed under different temperature-voltage stresses so that the relation of m value versus temperature and m value versus voltage could be obtained experimentally.

Fig.17 shows the I-t characteristics for X7R, Z5U and NPO capacitors at room temperature. The polarization currents decrease with time at different rate (different m value) for the different type of capacitor. The m value could be obtained from the slopes of each curve as shown in the following:

Sample	m Value
X7R	1.0
Z5U	0.8
NPO	0.5

Table 3. Some properties of three types of MLC capacitors

Capacitor Type	Nominal K	Capacitance	$BaTiO_3$ Content (%)	Nominal Grain Size (μ m)
NPO	100	56 pF	10 ~ 50	1
X7R	2000	100 nF	90 ~ 98	1
Z5U	5000	1 μF	80 ~ 94	3 ~ 20

(cont.)

Conductivity(25°C) ($1/\Omega \cdot$ cm) at t = 100 sec.	Temperature Range Sepcified	Maximum Capacitance Change Allowed
$6.4*10^{-15}$	-55 ~ +125 °C	± 30 ppm
$2.7*10^{-14}$	-55 ~ +125 °C	± 15%
$4.4*10^{-14}$	+10 ~ +85 °C	+20% ~ 56%

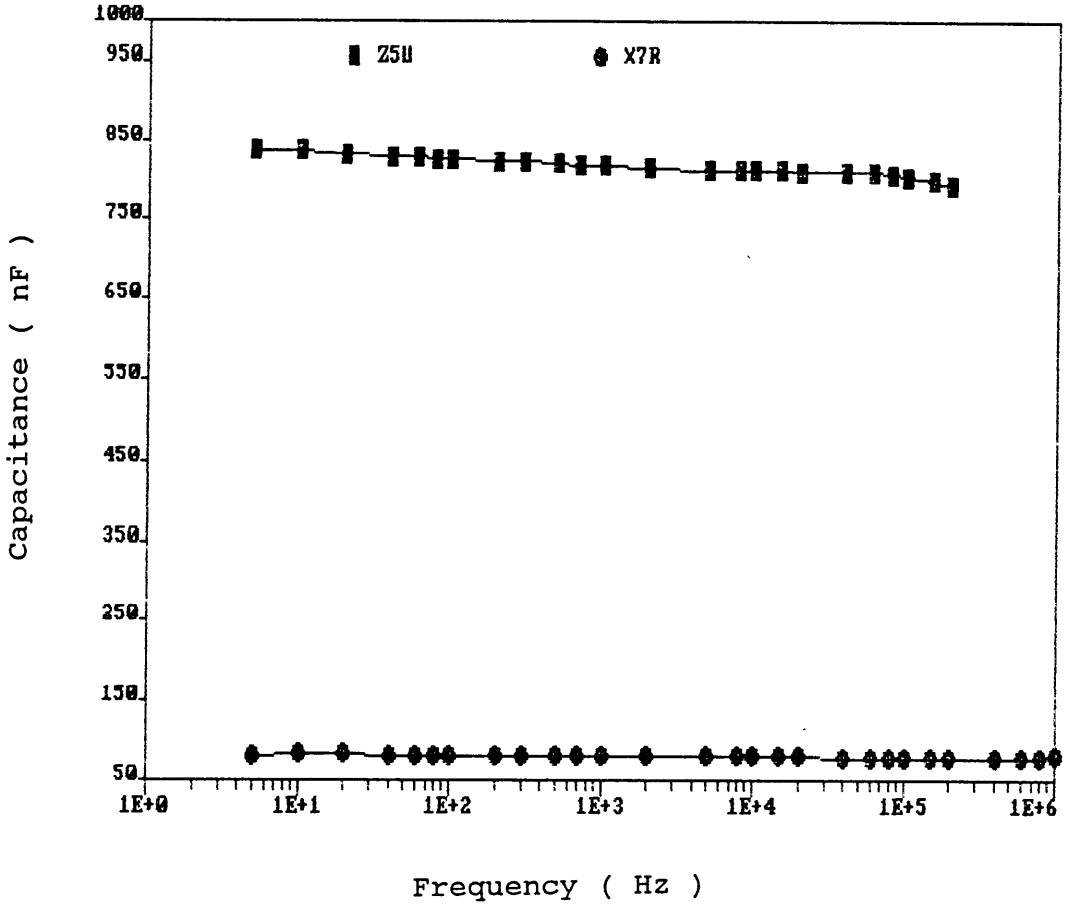

Figure 15. The frequency-dependence of the capacitance for X7R and Z5U at room temperature.

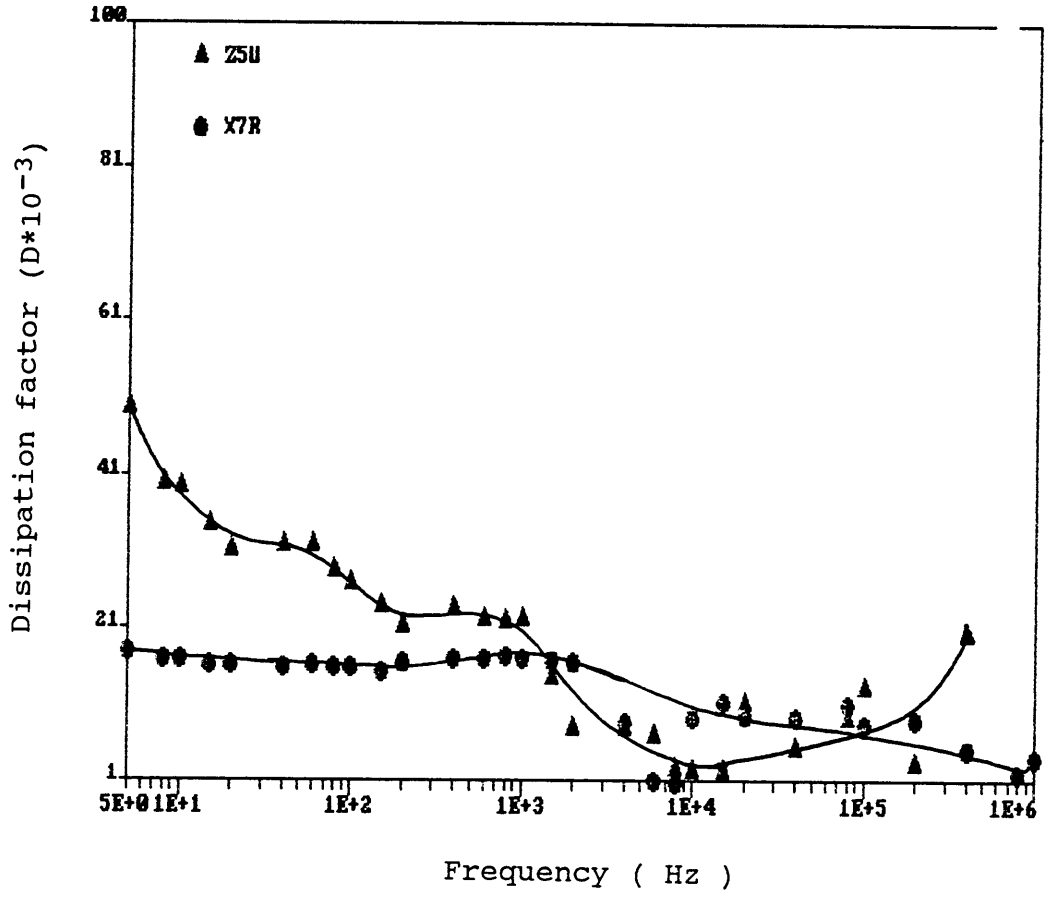

Figure 16. The frequency dependence of the dissipation factor for X7R and Z5U under 10 volts bias, at room temperature.

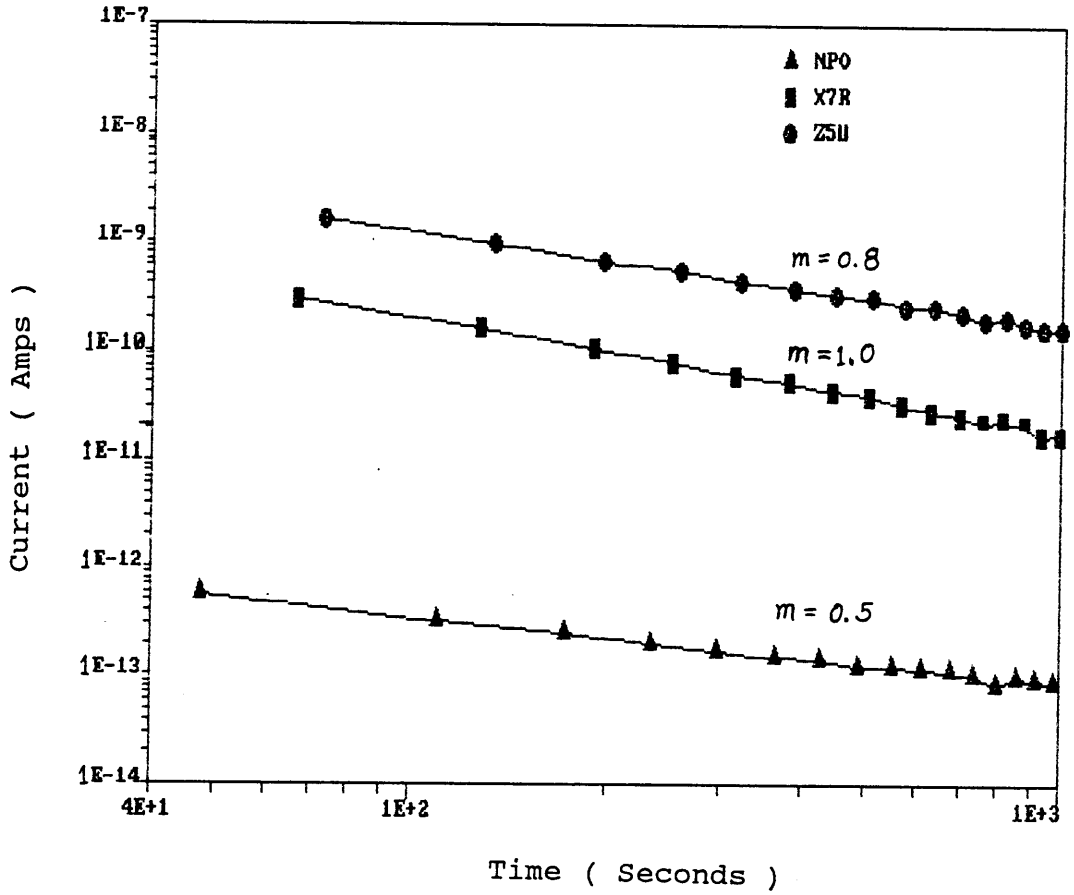

Figure 17. I-t characteristics for different types of ceramic capacitors at T = 25 ^{o}C and V = 10v.

The value of m provides valuable information about the material structure. In another words, the m value is determined by the structure of dielectric material. X7R and Z5U samples are ferroelectric MLC capacitors while NPO is a nonferroelectric type. Some properties of these samples are listed in Table 3[11,12,13].

The m value changes in different types of materials. In $BaTiO_3$-based ceramics, m value of ferroelectric, e.g. X7R and Z5U, is larger than that of nonferroelectric (NPO) because in ferroelectric there exist a large number of permanent dipoles. The dipoles are caused by charge carrier (electrons and ions) displacement, and then they can form domains in an internal field resulting in much higher polarizability in the ferroelectric materials below the Curie temperature[14].

Polarization also can be contributed by two types of hopping transitions ——— large and small transition that have been reviewed in Chapter 4. In ferroelectric materials, localized charge carriers may be displaced from their original positions by the action of an external field by means of short-range hopping transition between localized levels, not involving excitations into the respective free bands. This process indicates clearly that a hopping charge carrier shows both dielectric characteristics and conduction characteristics. The dielectric characteristics are evident as the hopping charge carrier behaves like a jumping dipole

in its reciprocating motions,and simultaneously conducting characteristics result from its extended hopping (long-range hopping) over many sites. The conducting hopping can be thermally excited.

These hopping motions, i.e. the short-range hopping which results in dipole presence and the long-range hopping which results in conduction, require energies typically on the order of 1 eV to take the charge carriers over the barriers hindering their motion in the lattice. This process is referred to as a large transition.

Another type of transition, i.e. the small transition, is the mutual slight rearrangement of charge carriers in a disordered system, according to a many-body interaction model[4]. This involves configurational tunnelling of a large number of particles including electrons (quantum mechanical tunnelling), which may be very heavy, e.g. ions, which make very small transition. This configurational tunnelling transitions of the flip and flip-flop types is temperature independent, and only depends on the number of interactions. The more the lattice is deformed, the more small transitions contribute to polarization process. However, the small transitions do not contribute to the conduction process.

An important property in this model is that the variation of the m value depends on how much the large transitions or small transitions contribute to the

polarization. If the large transitions contribute much more than the small transitions to polarization, the m value will becomes smaller. The m = 1 value corresponds to the lack of large transitions inside the materials.

The difference of the $BaTiO_3$ content and the grain size between X7R and Z5U capacitors is indicated in Table 3. It is observed that the structure of X7R is more disordered in bulk (due to inhomogeneously small grain in size and second phase or materials presence) than Z5U[5,12]. The small transitions are probably the predominant contributor to the polarization in X7R. Therefore, X7R capacitors show larger m value under the same I-t measurement conditions as Z5U. In contrast, the Z5U polarization is contributed by more large transitions. Thus Z5U capacitors show smaller m value and larger DC conduction current as illustrated in Fig.17.

The characteristics for temperature-dependence and for voltage-dependence of the m value are shown in Fig.18 and Fig.19, respectively. It is observed that the m value is more sensitive to the temperature than to the applied DC voltage. This phenomenon is related to the large hopping transitions, where the charge carrier hopping motions are strongly temperature dependent. Therefore, as the temperature increases, conduction current gradually dominates the total leakage current. This process lead to the decrease in m value, which has been discussed at the beginning of this section.

In order to investigate dielectric thickness effect on polarization behavior, the I-t measurements were performed by using a number of PLZT MLC capacitors with three different dielectric thicknesses (10 μm, 20 μm and 30 μm). Fig. 20 shows that the slopes are the same for all I-t curves. This concludes that the m value is independent of dielectric thickness. The dielectric thickness independence of m value at low voltages (V < 100 volts) has been proved by a set of I-t measurements. The m values for the three dielectric thicknesses PLZT samples are listed in Table 4.

6.2 Degradation Measurements

Studies were performed on the characteristics of the leakage current change with time, in order to evaluate the capacitor lifetime, by means of degradation measurements. Tremendous differences were found in degradation characteristics for different type of MLC capacitors under equivalent accelerated test conditions.

The degradation measurements were performed under elevated temperatures and at voltages several times higher than the rating voltage, i.e. under high temperature and high voltage stress. In the condition that the temperature is higher than 125 ^{o}C and DC applied voltage is higher than the rating voltage (50 volts), Z5U MLC capacitors tended to degrade exponentially with time. But the X7R MLC

Table 4. The m values for PLZT capacitors of three different dielectric thicknesses

Voltage \ T		25°C	50°C	75°C	100°C	125°C
2V	(1)	0.7219	0.9050	1.0283	0.8174	0.7180
	(2)	0.6743	0.8053	1.0060	0.7937	0.6778
	(3)	0.7126	0.9622	1.0597	0.8779	0.6410
5V	(1)	0.7371	0.9234	1.0070	0.8350	0.7024
	(2)	0.7112	0.9083	0.9949	0.8213	0.6593
	(3)	0.7512	0.9454	1.0307	0.8637	0.6186
10V	(1)	0.7561	0.9527	1.0000	0.8283	0.6874
	(2)	0.7001	0.9277	1.0016	0.8028	0.6572
	(3)	0.7266	0.9410	1.0293	0.8163	0.6337
20V	(1)	0.8290	1.0106	0.9373	0.8132	0.6725
	(2)	0.7586	0.9794	0.9205	0.7261	0.6419
	(3)	0.8097	0.9817	0.9522	0.7980	0.6337
50V	(1)	0.8707	1.0079	0.8410	0.6710	0.6210
	(2)	0.8426	1.0205	0.8633	0.7261	0.6419
	(3)	0.8103	1.0397	0.8814	0.7460	0.6247
100V	(1)	0.7788	0.6988	0.6273	0.4735	0.4251
	(2)	0.9319	0.8857	0.7871	0.6383	0.6598
	(3)	0.9558	0.9514	0.8518	0.6695	0.6476

(1) ----- PLZT AA-272 (10 micron thickness)
(2) ----- PLZT AA-273 (20 micron thickness)
(3) ----- PLZT AA-274 (30 micron thickness)

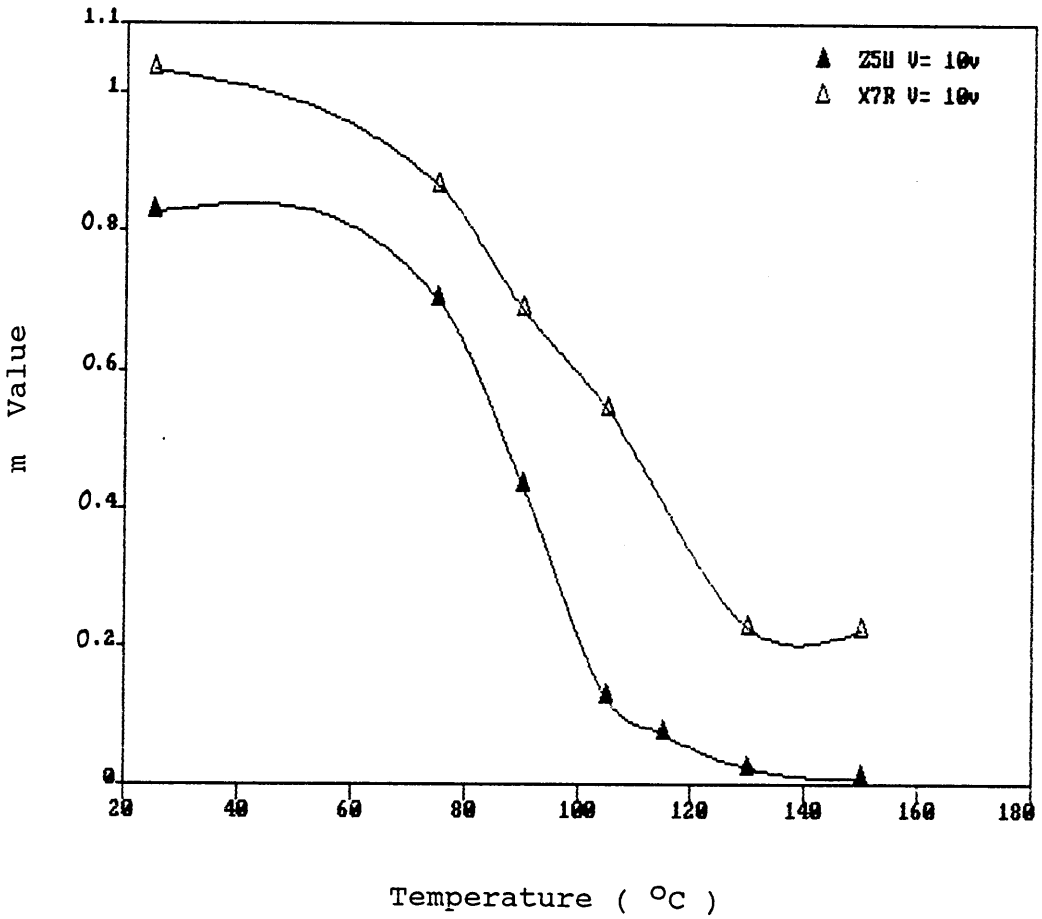

Figure 18. The m value versus temperature for both X7R and Z5U at V = 10 volts.

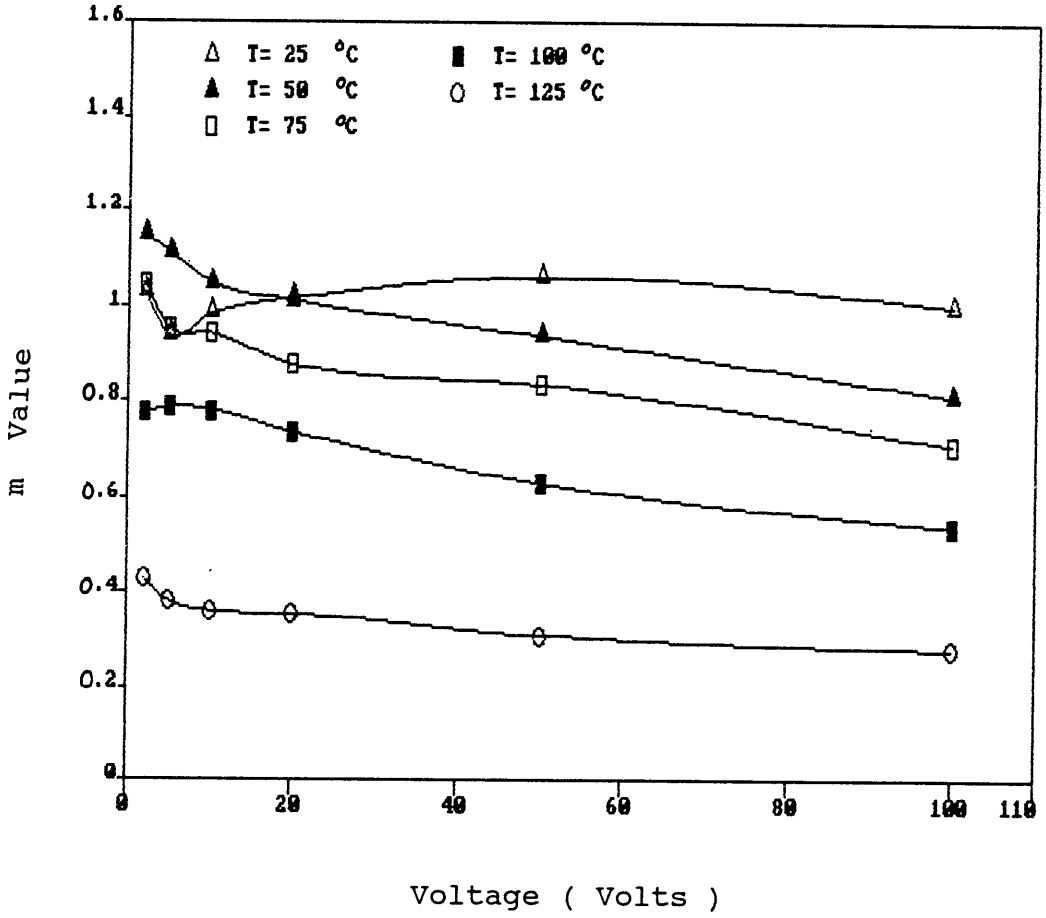

Figure 19. The m value versus applied voltage for X7R at different temperatures.

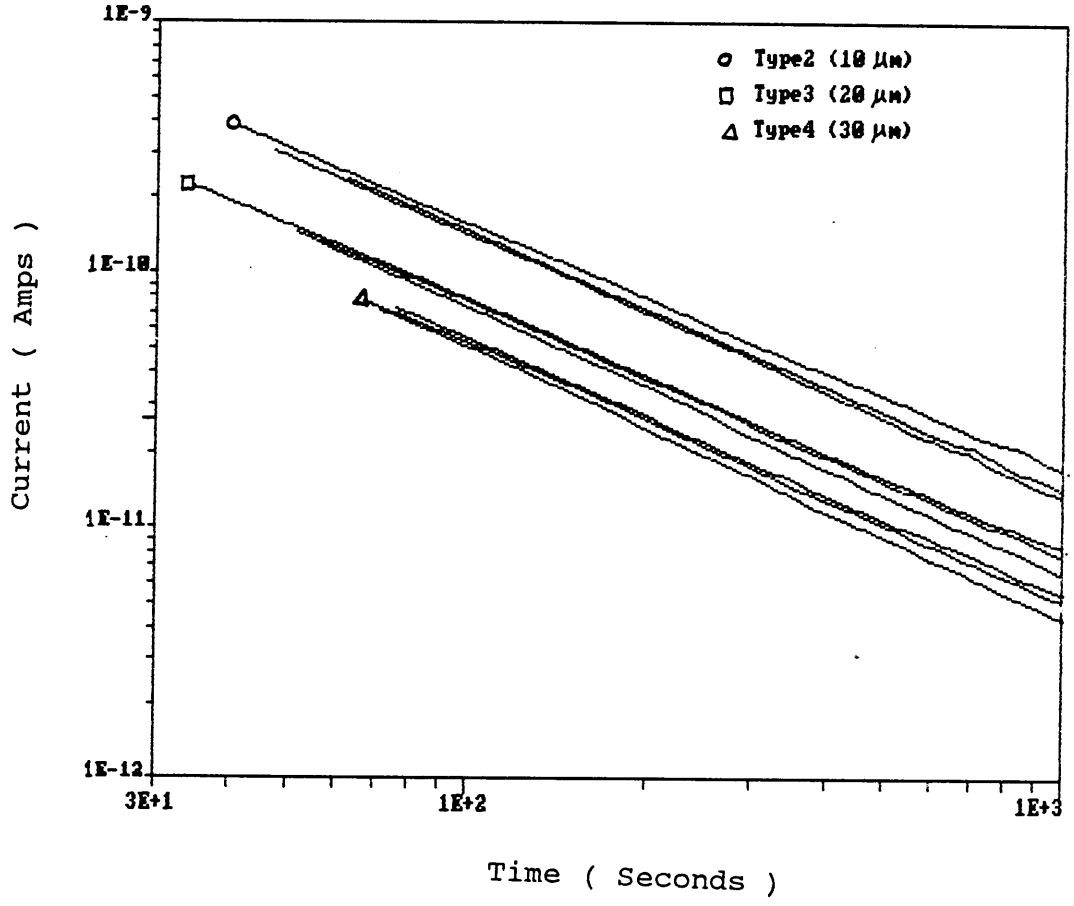

Figure 20. I-t characteristics for PLZT chips of different thickesses at T = 75 ^{o}C and V = 10 volts.

capacitors tested under the same condition showed no sign of degradation after a long period of time. The X7R MLC capacitors were found to degrade under higher accelerated test stresses. The X7R degradation showed that the leakage currents increased with time as a power law in the first stage, i.e. before a transit time t_o, and then they continued to increase with time exponentially. Such X7R degradation behavior can probably be partly explained by modifying the already developed degradation models[7,15], based on the phenomenon of electron injection into the ceramics.

The effects of polarity reversal on the degradation were also examined for both X7R and Z5U.

6.2.1 Z5U MLC Capacitor

Fig.21 shows I-t degradation characteristics of Centralab Z5U MLC capacitors (1 μF) at 50 volts and in the temperature range of 150 ^{o}C to 200 ^{o}C. The leakage currents increase with time exponentially at different degradation rates (β). The β value is defined as the slope of the I-t curve in a semi-log degradation plot. It is evident that the degradation rate increases with raising temperature.

The I-t degradation characteristics of the same type of Z5U capacitors, at constant temperature T = 175 ^{o}C and in DC voltage range from 50 volts to 200 volts, are shown in

Fig. 22. This result indicates that the degradation rate increases proportionally to the applied voltage.

The experimental results have shown that the lifetime τ , which is related to the degradation rate as $\tau = \beta^{-1}$, is inversely proportional to the exponential of temperature and to the nth power of voltage for Z5U type MLC capacitors. These results agree with the Minford model reported[16,17]. The mean lifetime τ for Z5U is described by

$$\tau \propto V^{-n} \exp [E_A / kT] \quad -------(6.10)$$

where E_A is an activation energy. n is a constant which only depends on capacitor composition. The relations of degradation rate β depending on DC voltage and temperature are shown in Fig. 23 and Fig. 24, respectively. The voltage-dependence and temperature dependence of degradation rate follow the relation (6.10) very well. Thus, n value was obtained from the slopes of the curves in Fig. 23. The n value for Centralab Z5U is about 1.9 $\pm$ 0.2. The activation energy E_A, obtained from the slopes of the curves in Fig.24, is about 1.25 $\pm$ 0.1 eV.

Studies on degradation for different types of MLC capacitors such as Z5U and X7R explored some interesting results that could reveal the possible degradation mechanisms. The degradation rate is determined by bulk

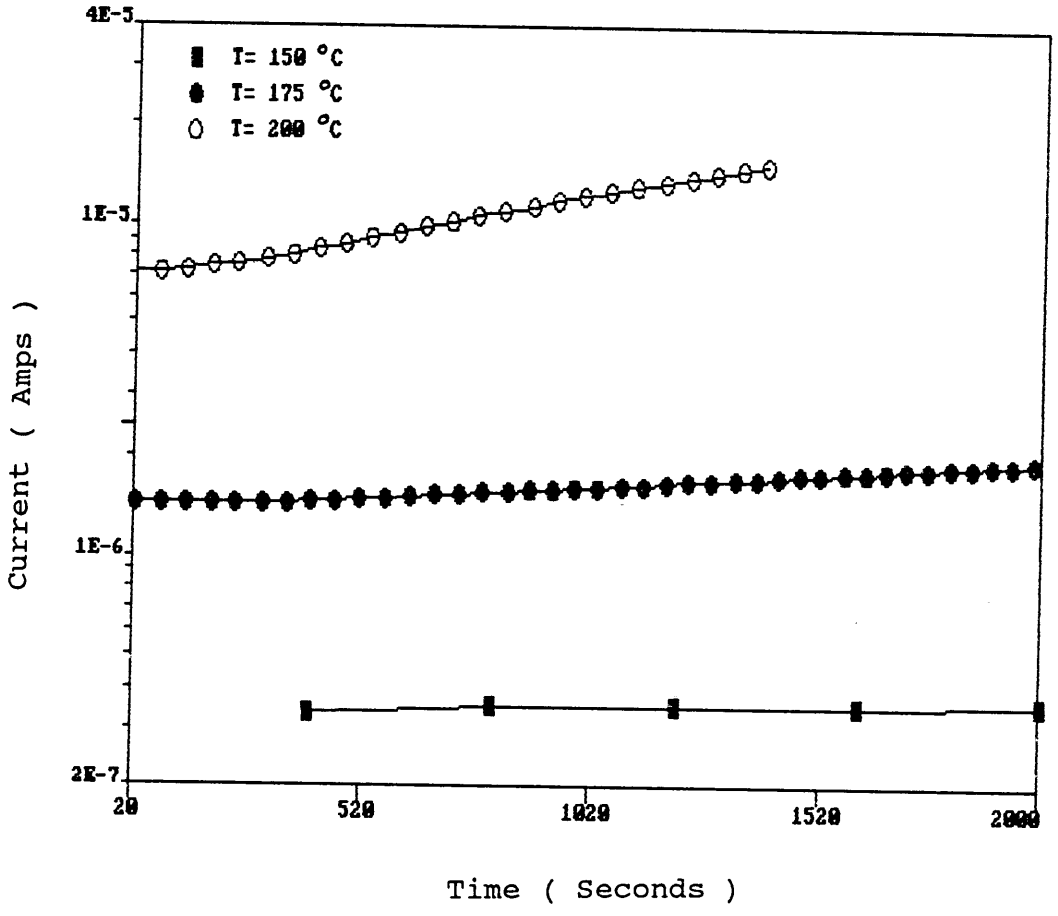

Figure 21. I-t characteristics for Z5U in degradation at different temperatures, at 50 volts.

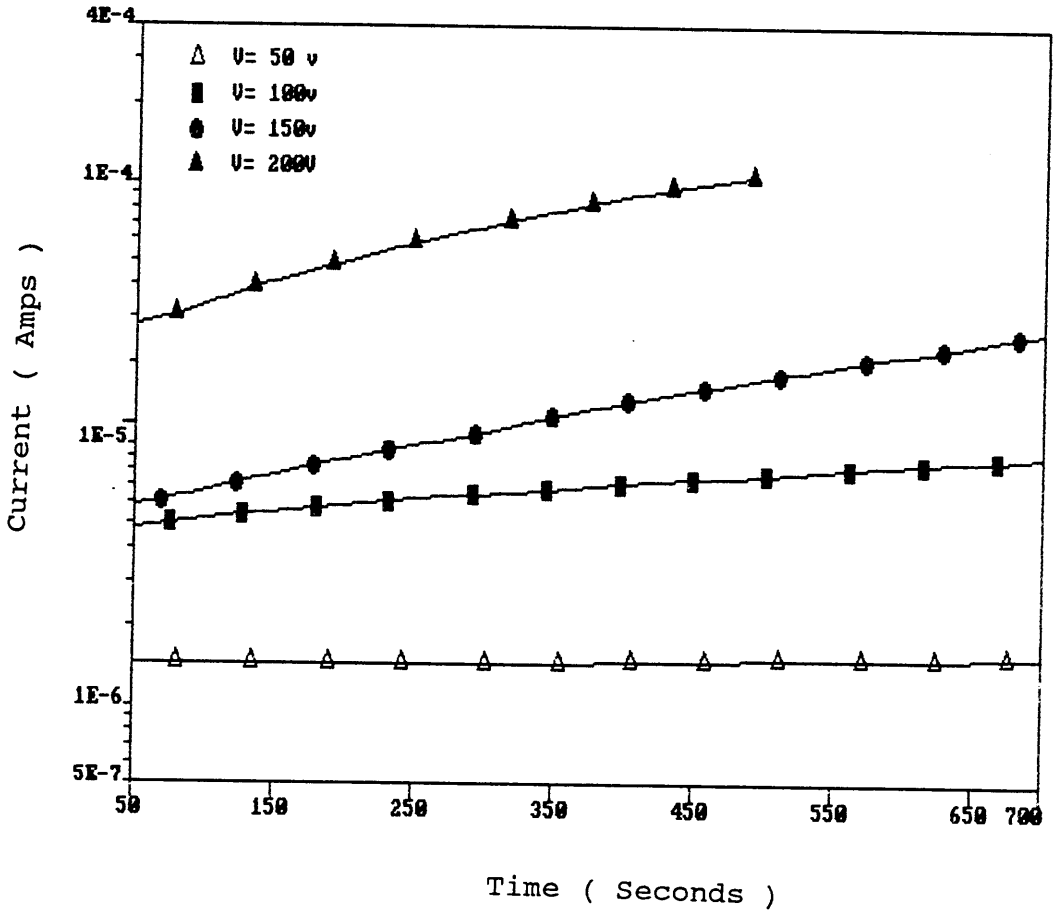

Figure 22. I-t characteristics for Z5U in degradation at T = 175 ^{o}C, and under different voltage stresses.

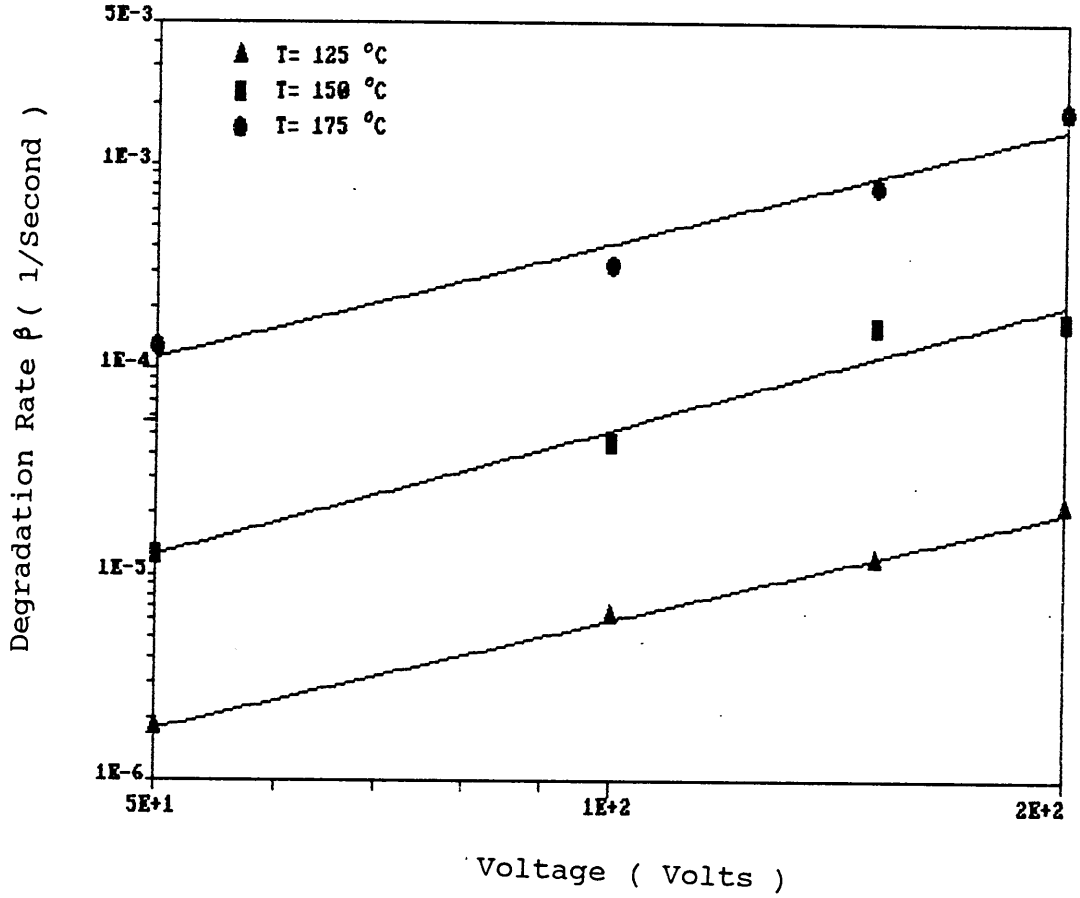

Figure 23. Voltage dependence of the degradation rate for Z5U at different temperatures. The power value $n = 1.9 \pm 0.2$.

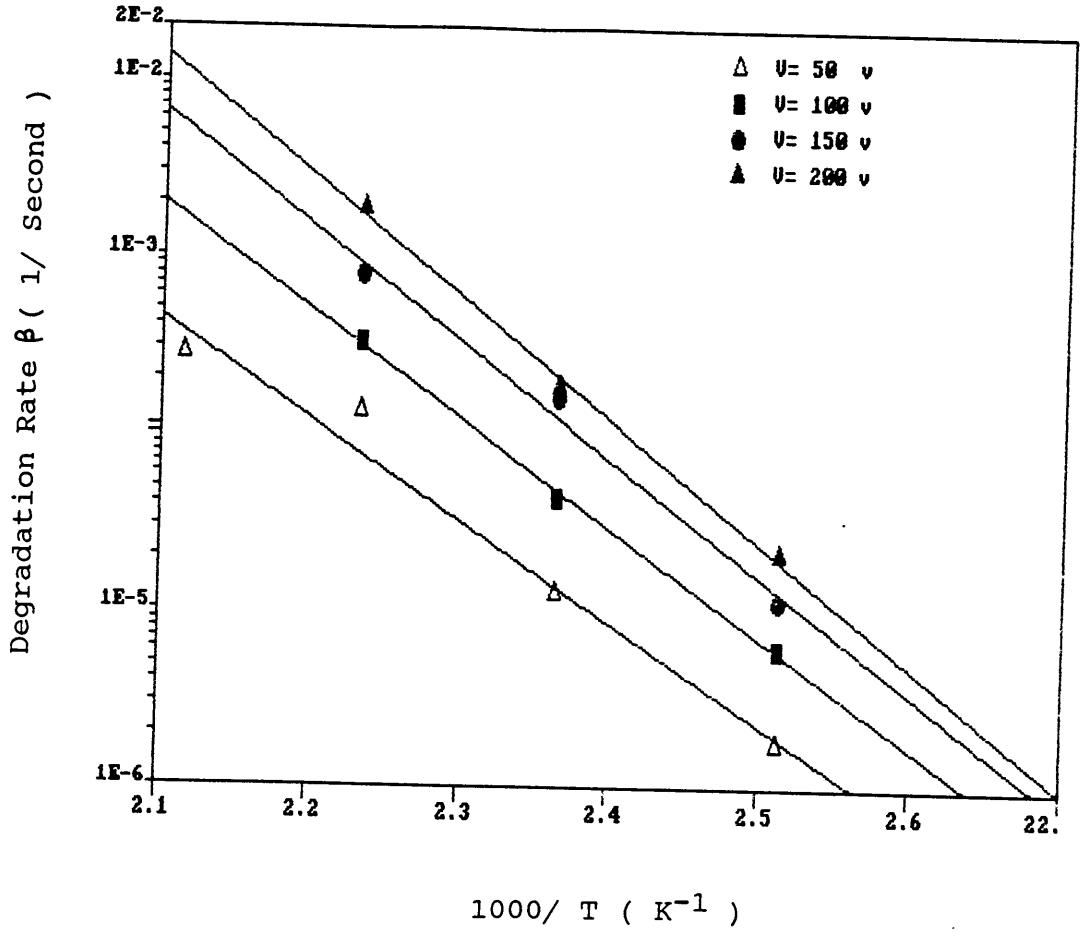

Figure 24. Arrhenius plot of temperature dependence of the degradation rate for Z5U at different voltages. Activation energy E_A = 1.25 ± 0.1 eV.

ceramic composition, grain size, grain shape, and electrode materials. The degradation rate is also very sensitive to the device process techniques such as doping, sintering temperature and atmosphere, sintering period, cooling rate, heat treatment, and electrode formation. A large number of factors contribute to the degradation behavior and it is necessary to determine which one of those dominates the others. In another words, which type of conduction transport is predominant factor in the device. Generally speaking, a few factors affect it simultaneously while one of them is more effective than the others.

At lest two possible degradation mechanisms that result in degradation in high-K and high resistance MLC capacitors can be considered[7]. One is a carrier concentration model in which oxygen vacancy generation enhances the carrier concentration while the other is a grain boundary model in which the reduction of grain boundary (GB) barrier height enhances the electron drift mobility. These two mechanisms may potentially both be present and coupled since GB barrier height depends on the donor density.

The exact role of GB in the impedance of high resistance ceramic has not been established. However, according to the experimental results, the grain boundary model possibly pertains to Z5U degradation, while the carrier concentration model may be more suitable to explain the X7R degradation, which will be discussed in detail in

the next section.

In a Z5U MLC capacitor the time dependent exponential increase in the leakage current, due to ionic conduction (oxygen vacancies) plus the increased electronic conduction, due to the decreasing stoichiometry, is termed here as "ionically induced current" I_d. I_d can be expressed based on the grain boundary model as

$$I_d = I_{do} \exp [\beta t] \quad \text{----------} \quad (6.11)$$

where β is the degradation rate and I_{do} is a constant. The conclusion that Z5U degradation can be modelled by the reduction of GB barrier height is based on the following facts:

(i) It is known that only Z5U MLC capacitors which failed by thermal runaway showed the signs of a color gradient in polarized reflected light[5,6]. A color gradient developed between the electrodes of opposite polarity is in itself a strong indicator of oxygen vacancy conduction. An identical phenomenon was found in PTC-type $BaTiO_3$ ceramics, which showed the flow of electric current across only closely connected grains[18]. SEM pictures showed that the grains of Z5U-type ceramics were polygonal in shape and in close contact with each other[5,12]. This is one reason why there exists a color gradient between the electrodes.

(ii) From the results of SEM analyses[5,12] for Z5U MLC

capacitors and Z5U density blanks, it is known that the grains of the Z5U-type materials are polygonal, approaching spherical in shape, and are fairly uniform in size, with most grains being 5 to 7 μm in diameter, which are much larger than that of X7R samples (up to 1 μm in diameter). As discussed in section 3.3, that the GB barrier height increases with increasing grain size due to decreased grain curvature[19].

(iii) SEM studies reveal that there is a very thin grain boundary between two grains (although excess oxygen and dopant atoms may be present). This means the depletion layer near the grain surface is very thin because there is a low concentration of oxygen vacancies near the grain surface and there is a high concentration of oxygen vacancies inside the grains. And the larger the grain size, the bigger the difference in oxygen vacancies concentration. Therefore, a GB barrier is formed by the negative charges trapped at GB with associated positive charges in the adjacent grains, which is shown in Fig. 25(a). When an external electric field is present, a higher electric field is applied to each grain boundary layer. It is expected that the electric field in the GB (actually the depletion layer near the grain surface) is about an order of magnitude higher than the average field across the grains[20,21,67,73].

Since such a high voltage is presented across the GB, it is proposed that there is a decrease or breakdown of GB

barrier in much the same manner as for zinc oxide varistors[22,23,32,33] or PTC $BaTiO_3$ ceramics[24,25]. It has been reported that the activation energy E_A value decreases with increasing voltage in Z5U and NPO, but not in X7R capacitors[7]. This voltage dependence of activation energy in Z5U may be due to reduction of GB barrier height. In this argument, the large grain size capacitors may show stronger Poole-Frenkel characteristics resulting in greater degradation rate under a voltage stress[29].

(iv) The well-known power relation between degradation rate of Z5U and the applied voltage, i.e. $\beta \propto V^n$, is due to the intrinsic dielectric failure processes. This is because of the electric-field-assisted thermal ionization of trapped charge carriers, as well as the electrostriction effect in GB region which are both characterized by the reduction of GB barrier height[16,21,28]. This intrinsic failure behavior is characterized by thermal runaway (TRA)[26,27]. In the degradation measurements, the Z5U capacitor failed via TRA by self heating that was caused by the almost gradual increase of the leakage current magnitude, as shown in Fig. 26(a). In contrast, as shown in Fig. 26(b), the leakage current in X7R capacitor shows a discontinuous rise because of the extrinsic dielectric failure processes which is termed avalanche breakdown (ABD). The ABD indicates the failure due to extrinsic defects present in the material.

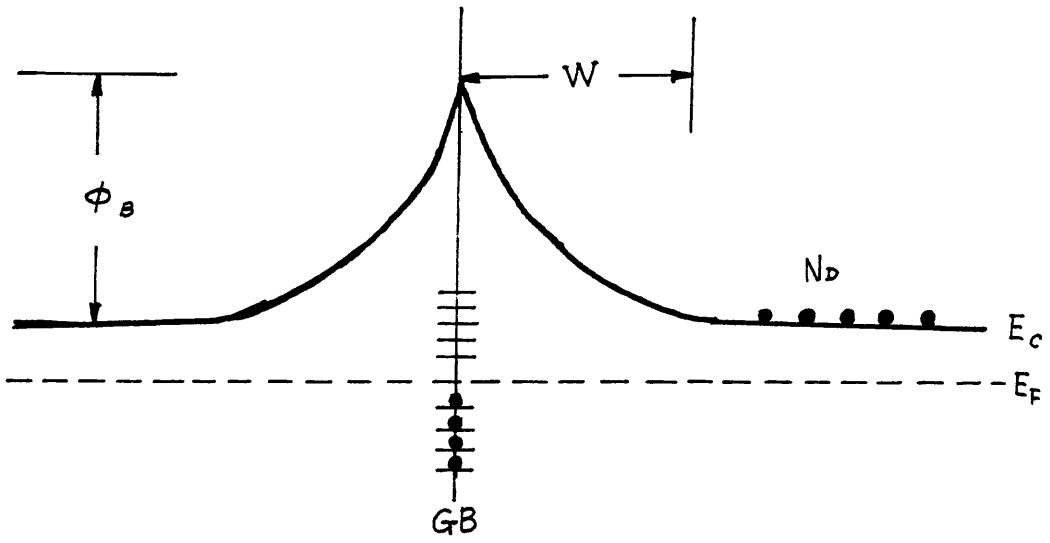

Figure 25(a). GB potential energy diagram for negative charge trapped at GB for Z5U ceramic.

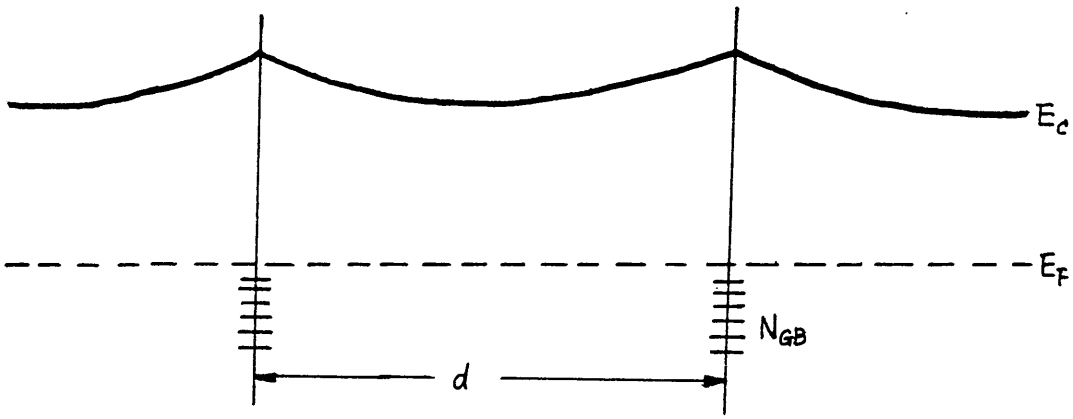

Figure 25(b). GB potential energy diagram with high GB state density N_{GB} near GB in X7R ceramic.

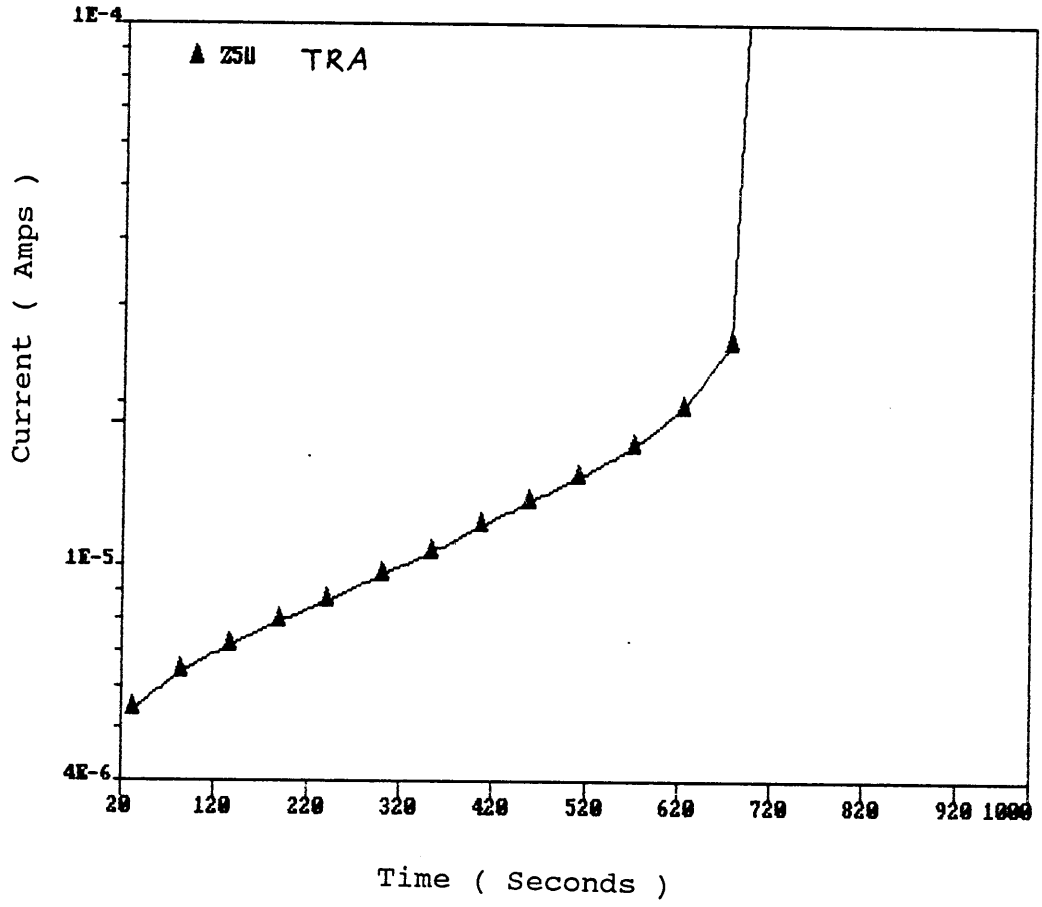

Figure 26(a). Leakage current as a function of time for Z5U at T = 175 ^{o}C and 100 volts.

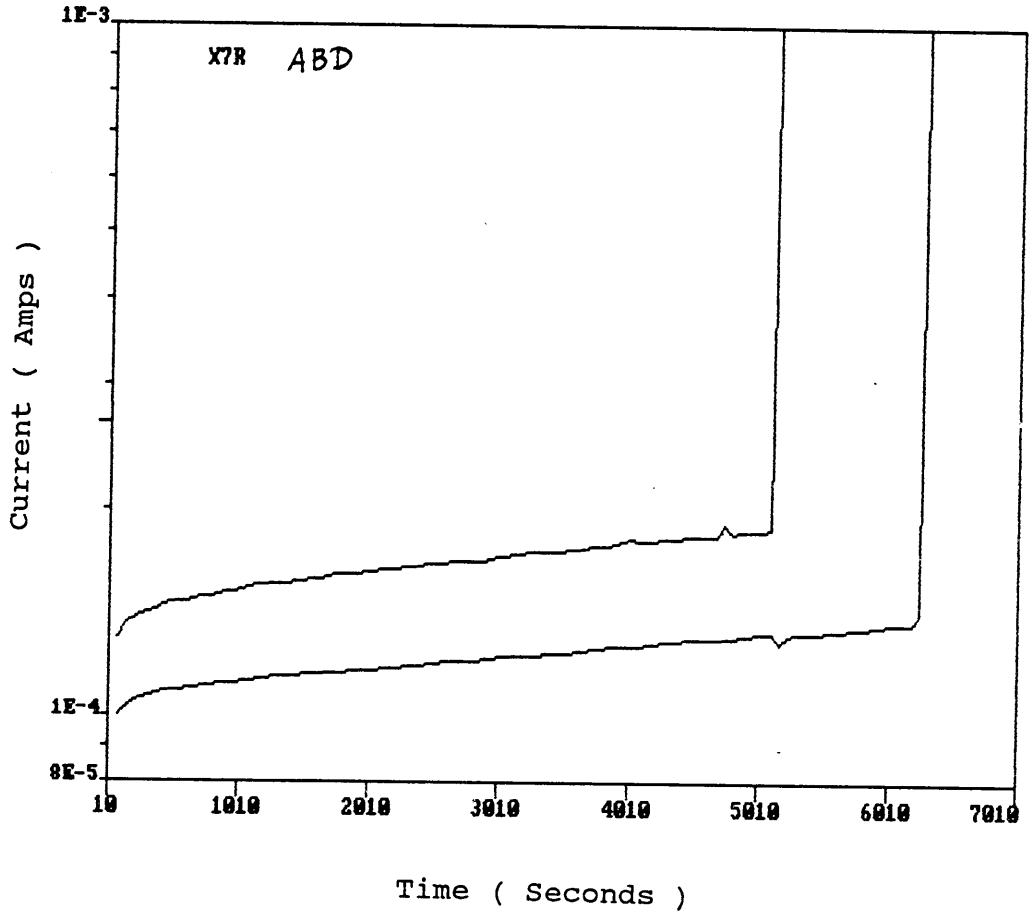

Figure 26(b). Leakage current as a function of time for X7R at T = 274 ^{o}C and 200 volts.

In summary, the degradation mechanisms for Z5U MLC capacitors can be explained by a reduction of GB barrier height. The leakage current can be expressed as

$$I_d = I_{do} \exp [- E_A / kT] \quad \text{--------} \quad (6.12)$$

Based on the GB model discussed in Reference (15), the activation energy E_A is best expressed in terms of a GB potential barrier height ϕ_B. Then Eqn. (6.12) becomes

$$I_d = I_{do} \exp [- \phi_B / kT] \quad \text{----------} \quad (6.13)$$

The barrier height ϕ_B follows the relation

$$\phi_B = \phi_{Bo} - A t \quad \text{----------} \quad (6.14)$$

where ϕ_{Bo} is the barrier height without applied voltage, and A is a constant. Thus combining Eqn.(6.13) with Eqn.(6.14), the result shows the leakage current increases exponentially with time as expressed in Eqn.(6.11).

Any error for using this model in high-K and high resistance Z5U type capacitors is probably due to the first two assumptions, which may not always be true for those inhomogeneous ceramics.

6.2.2 X7R MLC Capacitor

Fig. 27 shows the I-t degradation characteristics of X7R MLC capacitors (100 nF). The I-t curves under high temperature and high voltage stress are plotted on both log-log scale and semi-log scale in fig. 27 (a), and (b) respectively. It is observed that the leakage currents increase with time as a power law during the first stage when t < 1500 seconds, and then they continue to increase exponentially when t > 1500 seconds. The degradation rate β here is defined by the slope of the curve in the exponential I-t relation section as shown in Fig. 27(a).

Regarding the results obtained from the degradation measurements, we found that β for X7R is much smaller than that for Z5U, even under much higher accelerated conditions. The β value for X7R increases with increase in temperature and DC voltage similar to the I-t characteristics as shown in Fig.28 and Fig.29, respectively.

From the experimental results for X7R, the Minford's model accounts only partly for the relationship between lifetime τ ($\tau = 1/\beta$), and temperature and voltage. The temperature dependence of β is shown in Fig.30. The change of β follows Arrhenius behavior over a limited temperature range from 225 ^{o}C to 283 ^{o}C in region 2. This can be expressed as $\beta \propto \exp[-E_A/kT]$, where E_A = 1.31 eV in X7R.

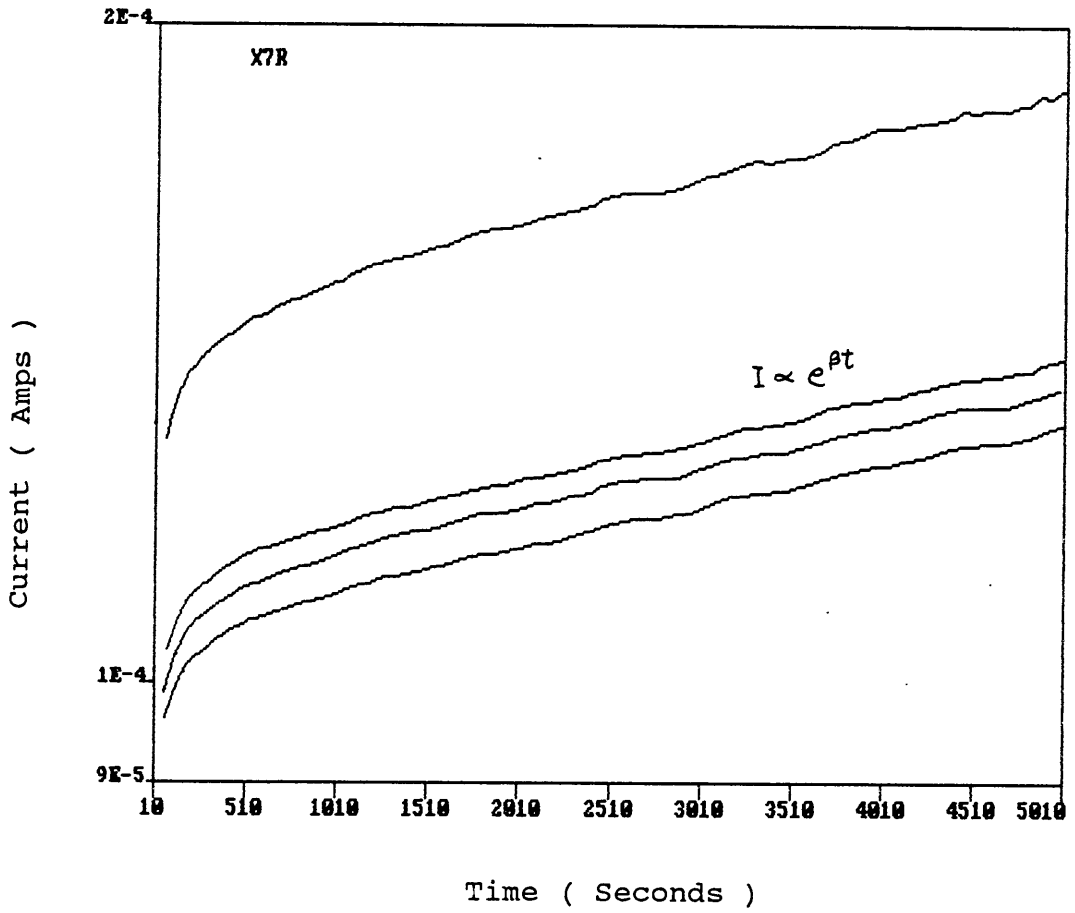

Figure 27(a). I-t characteristics for degradation on a semi-log plot for X7R at T = 265 ^{o}C and 200 volts.

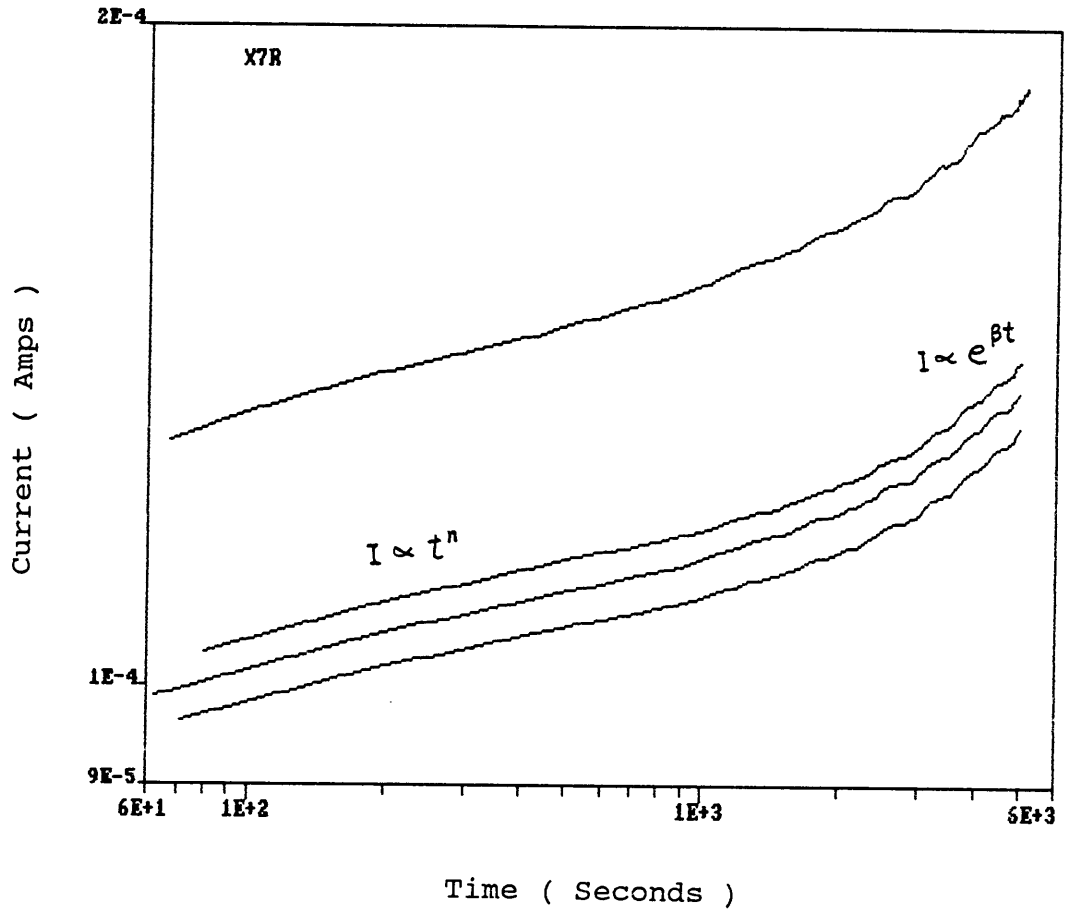

Figure 27(b). I-t characteristics for degradation on a log-log plot for X7R at T = 265 ^{o}C and 200 volts.

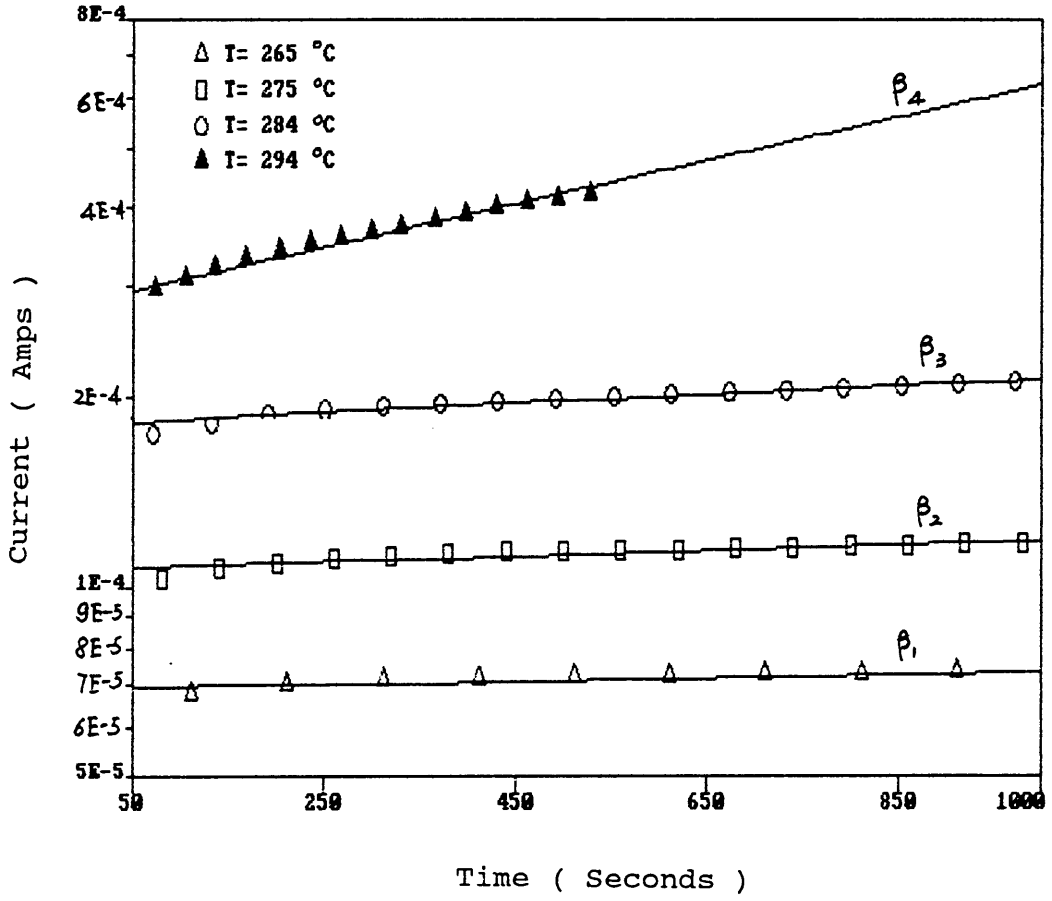

Figure 28. I-t curves of degradation for X7R at different temperatures, and 200 volts. β = slpoe.
$\beta_1=2.73*10^{-5}$; $\beta_2=4.32*10^{-5}$; $\beta_3=6.91*10^{-5}$;
$\beta_4=3.47*10^{-4}$.

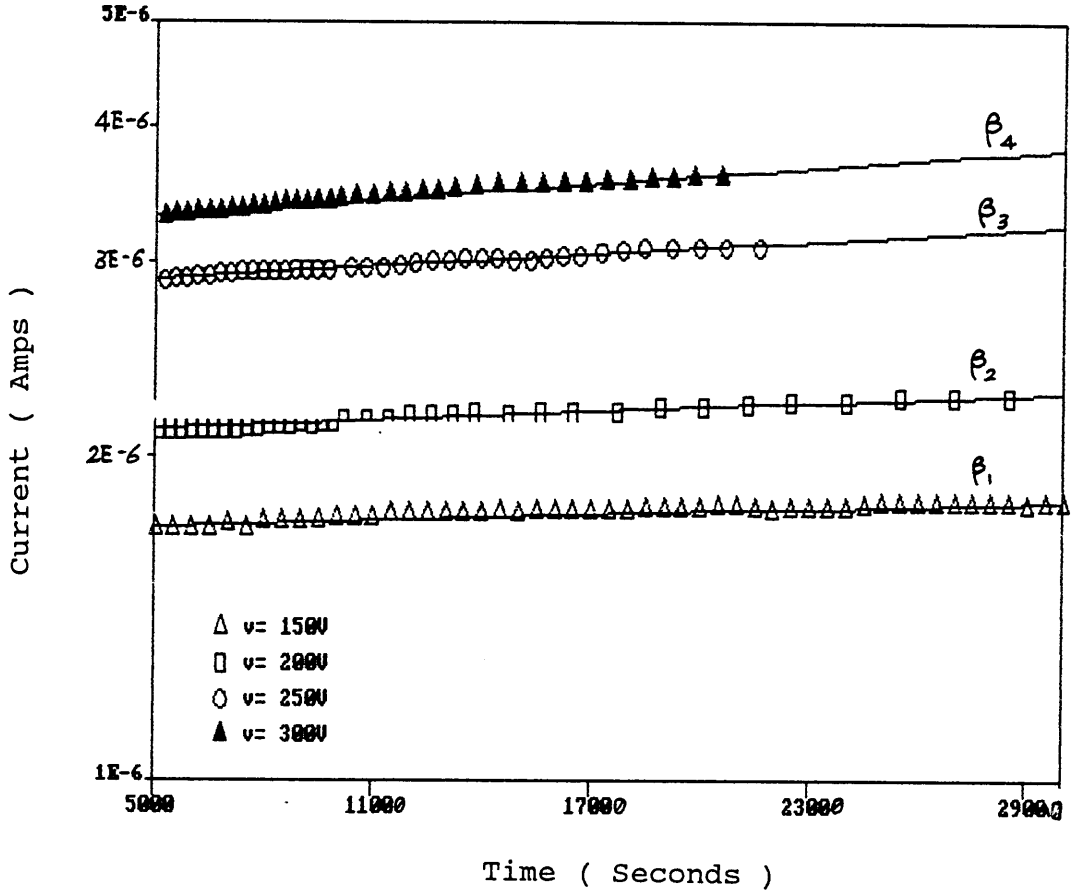

Figure 29. I-t curves of degradation for X7R at T = 217 ^{o}C and under different voltage stresses. β = slope. $\beta_1=8.80*10^{-7}$; $\beta_2=1.27*10^{-6}$; $\beta_3=1.90*10^{-6}$; $\beta_4=2.44*10^{-6}$.

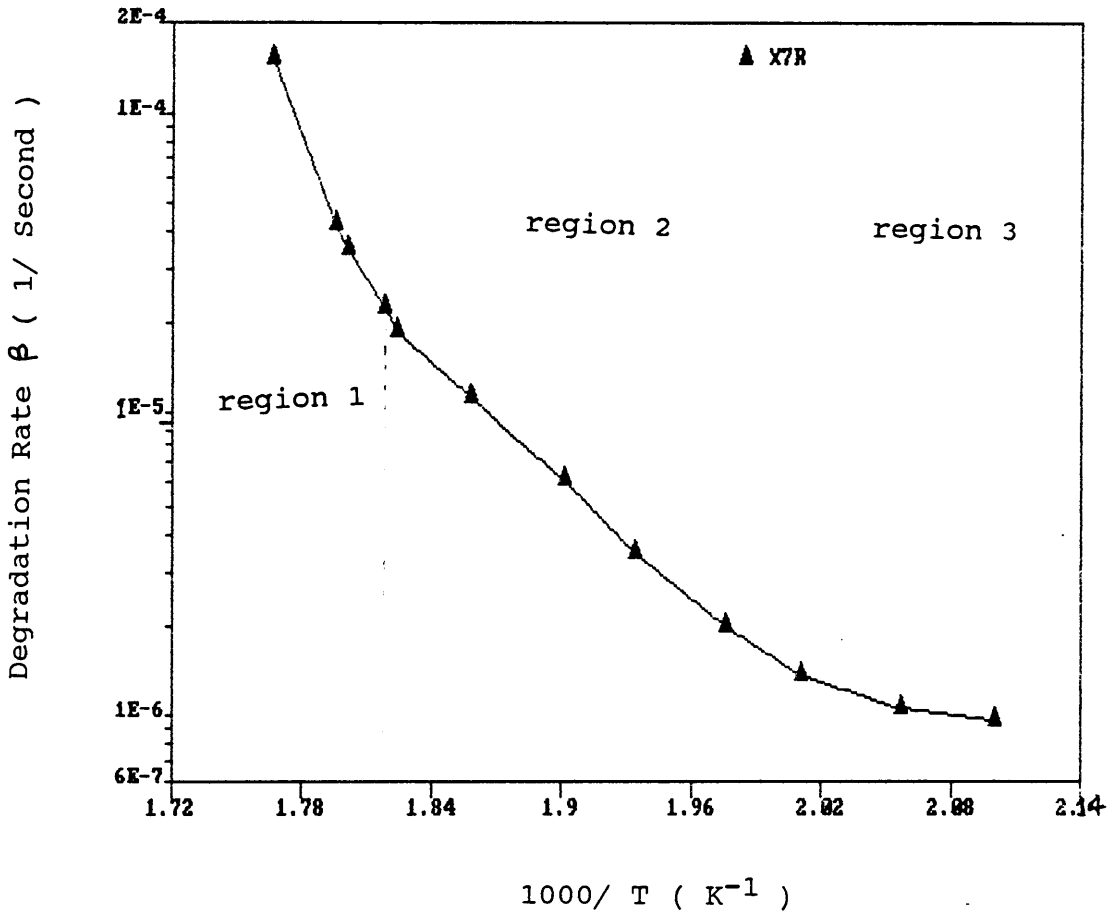

Figure 30. Arrhenius plot of temperature dependence of the degradation rate for X7R at V = 200 volts. Activation energy in region 2 is E_A = 1.31 eV.

In region 3 (T < 225 ^{o}C) the mechanism of field distribution with time, which corresponds to space-charge-limited current, possibly predominated the conduction transport inside the X7R capacitor[45,46]. In region 1 (T > 283 ^{o}C) the capacitor failure modes is present in the conduction processes[30]. These failure modes occur more or less instantaneously if the critical temperature or voltage values are exceeded.

Fig. 31 shows that the degradation rate of X7R increases exponentially with the increase in applied DC voltage, that is $\beta \propto e^{\alpha V}$. This characteristic can be attributed to field-assisted diffusion of "detrimental" ions in a high field. According to references (16) and (28), has the following dependence on voltage V and temperature T:

$$\beta = B \{ a \sinh(\alpha V) \} \exp[- H/kT] \text{ ------ } (6.15)$$

where a and B are constants determined by materials, and H is the potential barrier height for diffusion ions to overcome. The parameter in Eqn.(6.15) is defined as[28]

$$\alpha = \frac{qs\ E_e}{kT}\ \frac{1}{V} = \frac{q\ s}{kT}\ \frac{E_e}{E_a}\ \frac{1}{W}$$

where q is the electrical charge of the "detrimental" ion,

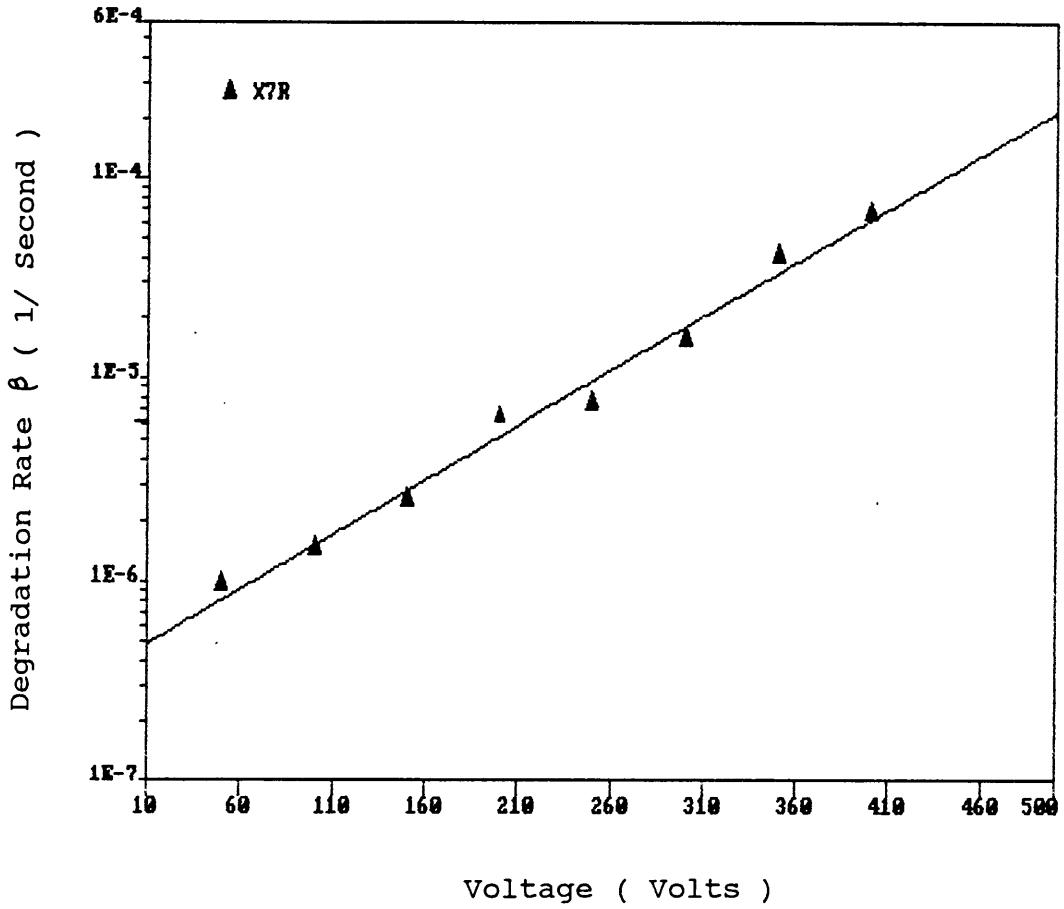

Figure 31. Voltage dependence of the degradation rate for X7R at T = 253 ^{o}C. Slope = α = 5.4*10^{-3}.

s is its half-jump distance, E_e is the local effective electrical field on the drifting ion when an external average filed E_a=V/ W applied to the capacitor with dielectric thickness W at the absolute temperature T, and k is Boltzmann's constant. For high field approximation of Eqn.(6.15), the relation $\beta \propto e^{\alpha V}$ is obtained.

This exponential voltage dependence of β may result in the extrinsic dielectric failure of X7R, which exhibit avalanche breakdown (ABD) behavior as shown in Fig.26(b). Since the probability of failure appears to rise exponentially with increasing voltage, which was found by plotting the statistical failure analysis data[5,26,31,34], the experimental results showing X7R ABD-like failure agree with the results of the above lifetime statistical analysis.

Thus, it is concluded that the failure is proceeded by $I \propto e^{\beta t}$ degradation for X7R capacitors. The lifetime for X7R is then described as

$$\tau = \beta^{-1} \propto \exp[- \alpha V + E_A/kT] \quad \text{---------- (6.16)}$$

where α is the exponent coefficient. Compared with Minford's expression [Eqn.(3.8)] for Z5U type capacitors, the relative lifetime for X7R can be described as

$$\frac{\tau_1}{\tau_2} = \exp[\alpha (V_2 - V_1) + E_A(\frac{1}{T_1} - \frac{1}{T_2})] \quad \text{---(6.17)}$$

The I-t power law behavior in the early stage was observed ($t < t_o$), which was followed by an exponential increase in leakage current with time, in the X7R degradation measurements. The possible mechanisms are explained below.

It has been found that electronic conduction predominates in X7R type barium titanate based ceramic as well as $BaTiO_3$ single crystal at temperatures lower than 500 ^oC[7,35,36,39]. In a $BaTiO_3$ single crystal the electronic conduction results have been interpreted in terms of small polaron hopping[37,38].

X7R ceramics were sintered with a controlled inhomogeneity in order to increase the stability[13]. The SEM analyses for X7R ceramic and capacitor materials reveal that there are extremely fine grain sizes in nearly spherical shapes that are up to 1 μm in diameter. The grains are surrounded by a continuous matrix of a second phase[5,12]. Therefore, a schematic energy diagram for X7R can be described as that shown in Fig.25(b). The reduction of GB barrier height occurs with a decrease in grain size because the grains became totally depleted of mobile charge, that is the charges in the grains can no longer compensate for the charge at the grain boundaries. It is expected that this kind of energy band structure will be less sensitive to the applied voltage since the band is "clamped" by the total depletion[10,69]. The experimental results show that the

activation energy value (E_A) for X7R ceramic and MLC capacitors are independent of bias voltages, while E_A decreases with increasing voltage in Z5U and NPO[7]. All these characteristics of microstructure in X7R may result in insignificant GB potential barrier effect in charge carrier transport.

Another reason that leads one to believe that the GB may not play a significant role in charge carrier transport in X7R is that the single crystalline and ceramic $BaTiO_3$ materials have a similar thermal activation energy[40]. The carrier transport in both materials is more likely due to the same mechanism, possibly small polaron hopping.

There might be other transport mechanisms in X7R which should not be excluded, such as large density of GB states, smaller electron capture and a higher resistivity region near GB[10]. In conduction mechanisms, space charge limited current has been seen in single crystal barium titanate[41,42,43], while evidence of double injection has been found for polycrystalline $BaTiO_3$[44].

Considering the characteristics of the increase in leakage current with time for X7R MLC capacitors based on the discussion above, the initial current in the early stages that increases with time as a power law, i.e. $I = I_1 t^n$, where I_1 is a constant, and the exponent n is dependent on the material, temperature and voltage. The n value lies in the range $0 < n < 1$. This power law relation

with time may indicate the injection of a high conductivity region from the cathodes, due to migration of oxygen toward the anode.

Then in the succeeding stage, an ionic induced (oxygen vacancies) conduction process plays an important role, which shows that the leakage current increases exponentially with time, i.e. $I = I_2 e^{\beta t}$, where I_2 is a constant, and β is the degradation rate.

For X7R at elevated temperatures, immediately after an application of DC voltage, the net space charge would be due to the electrons injected from the cathodes, since the charge of ionic species would still be balanced at each part of the dielectric. The picture of microscopic cross-sections of X7R capacitors shows some voids in dielectric layers with electrode metal, and also shows the roughness of the electrode surface to dielectric. This electrode protuberance is a potential source of enhanced electron injection. Also, Fig. 32(b) shows the I-V relation for a X7R MLC capacitor which indicates that the I-V curve transits from Ohmic ($I \propto V$) to space charge ($I \propto V^{1.27}$), while I-V relation for a Z5U shows an Ohmic behavior, as illustrated in Fig.32(a).

Electron injection from the cathodes would cause the piling up of an excess negative space charge leading to a high conductivity region near the cathodes, which is associated with the presence of trapped electrons in oxygen vacancies or impurities between two grains. It is proposed

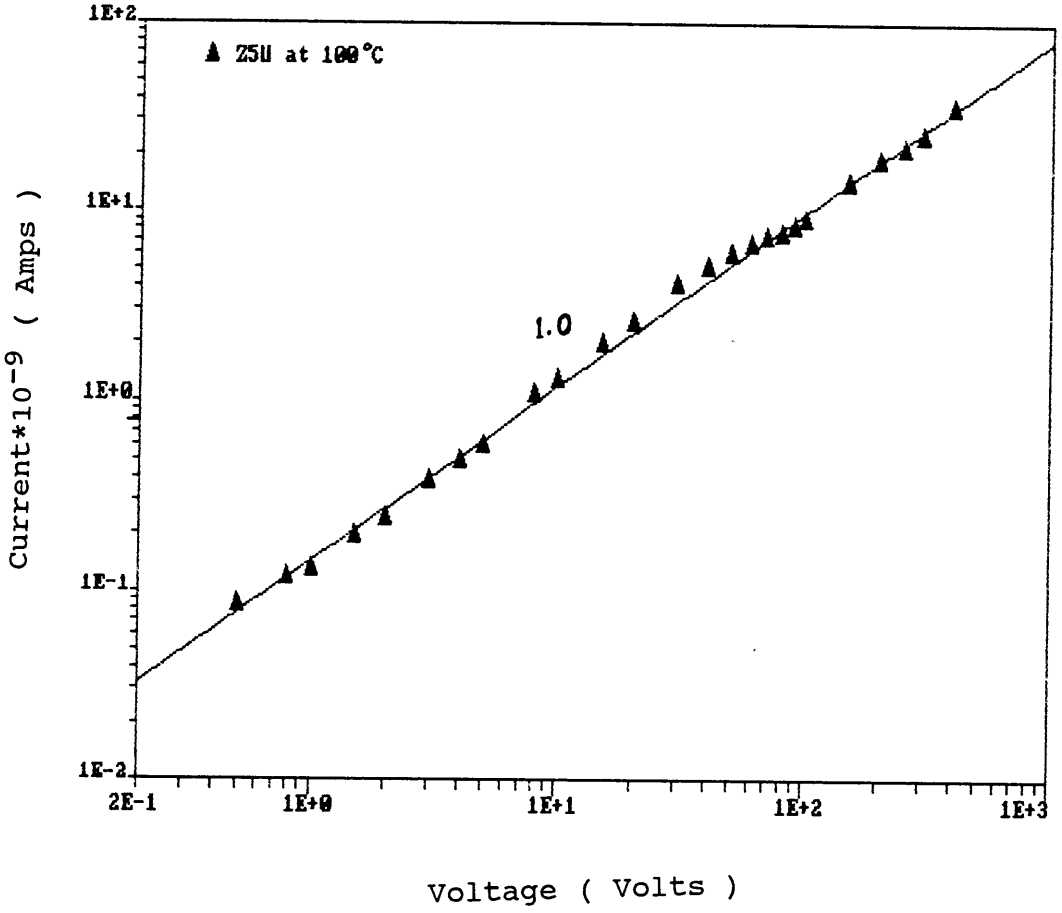

Figure 32(a). Ohmic I-V characteristics for 1 μF Z5U at T = 100 °C.

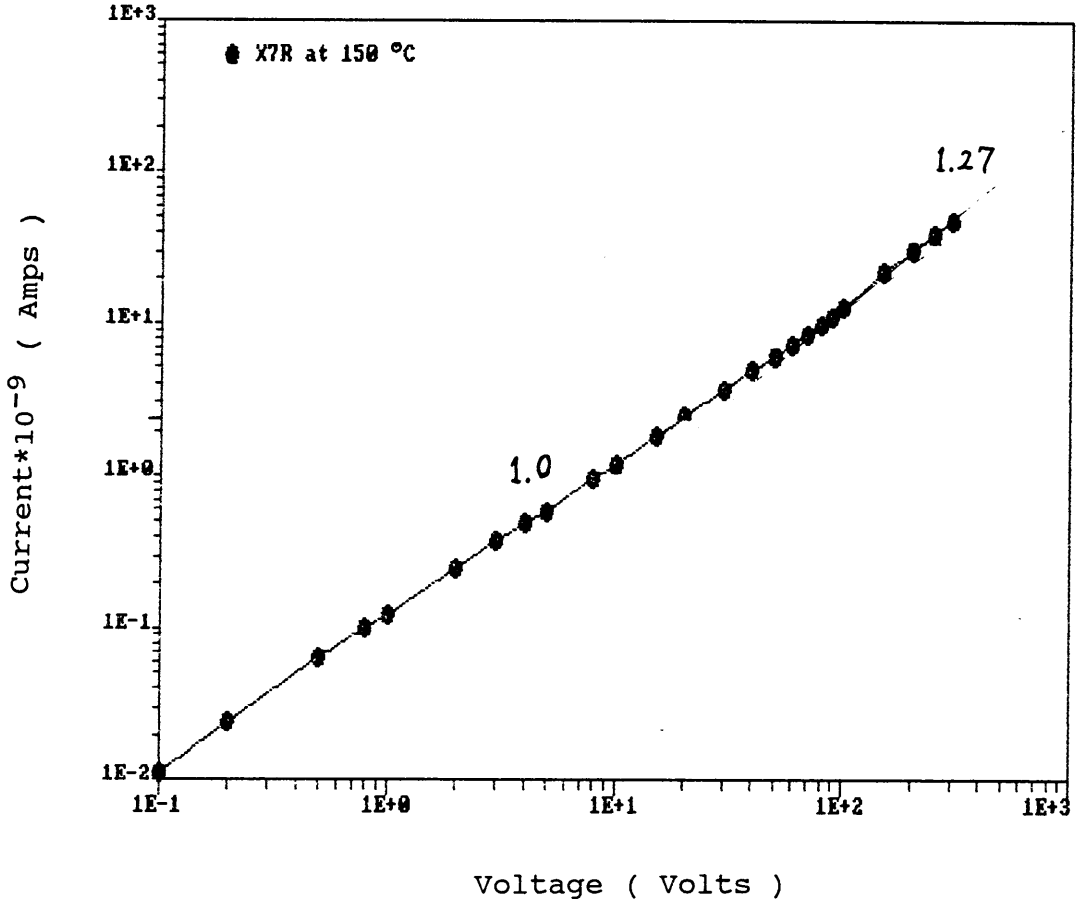

Figure 32(b). I-V characteristics for 100 nF X7R at T=150^{o}C.

that the thickness of the high conductivity layer at the cathode would become thicker with time. This thickness x grows with time according to a parabolic law[47,53]

$$x = b\ t^{1/2} \qquad \text{---------- (6.18)}$$

where b is a materials dependent coefficient. x is also the distance from cathode.

It has been reported that electrical conduction in the $BaTiO_3$ crystal or ceramic was not spatially homogeneous[45,46]. In the early stage of the conduction, the net space charge distribution curve is hyperbolic[46], which suggests the conduction is space-charge-limited. Therefore, the electric field in the dielectric layer can be obtained by using Poission's equation

$$\frac{dE(x)}{dx} = -\frac{4\pi\rho(x)}{K\varepsilon_0} \qquad \text{--------- (6.19)}$$

where ε_0 is permittivity in vacuum; K is dielectric constant and $\rho(x) \approx 1/x$ is the net space charge density.

It is suggested that the electric field strength in the dielectric in the early stage (when $t < t_o$) is distance and time distributed, and the electric field strength is nearly uniform in dielectric layer after a certain period of time t_o. The transit time t_o is defined as

(a) the time when the leakage current increasing with time in power law transforms into an exponential law; or

(b) the time when the electric field is assumed uniform in the dielectric layer; or

(c) the time when space-charge-limited current transforms to ionic induced current.

So the electric field strength can be expressed, by using Eqn.(6.19), as

$$E(x) = \begin{cases} a \ln x & \text{when } t < t_o \\ E = \dfrac{V}{W} & \text{when } t > t_o \end{cases} \qquad \text{------(6.20)}$$

where a is a constant, V is the applied DC voltage, and W is the thickness of each dielectric layer of the MLC capacitor.

(a) Considering the space charge limited current (SCLC) in the early stage when $t < t_o$, for a dielectric volume of cross section A and thickness W, the electronic current I_e can be expressed in two forms

$$I_e = qWA \ (dn_e/dt)$$

$$I_e = qA\mu_e E(x) n_e$$

where n_e —— electron concentration;

q —— electron charge;

μ_e —— electron drift mobility;

E(x) —— electric field strength.

Thus

$$\frac{dn_e}{dt} = \frac{\mu_e E(x)}{W} n_e \qquad \text{---------(6.21)}$$

By using Eqn.(6.18) and (6.20), we obtain the time dependence of the electric field

$$E(x) = a \ln(t^{1/2}) + C \qquad \text{-------(6.22)}$$

where a is the same constant as that in Eqn.(6.20), and C is a constant. Combing Eqn.(6.22) with Eqn.(6.21) and integrating Eqn.(6.22), the time dependence of electron concentration can be described as

$$n_e(t) = [\, n_e(0)\ t^{1/2}\ ]^{ct} \qquad \text{--- (6.23)}$$

where c=a μ_e/W is a material dependent constant (electron drift mobility μ_e is assumed not to change with time in the early stage), and $n_e(0)$ is the electron concentration at $t = 0$. In the condition that c=a μ_e/W is sufficiently small and t is small ($t < t_o$), (i.e. $a\mu_e t/W < 1$), the power term (ct) can be treated as a constant, M < 1. Then Eqn.(6.22) can be expressed

$$n_e(t) = n_e(0)\ t^n \quad \text{where } n = 1/2 < M \qquad ---(6.24)$$

Hence in the early stage, the conductivity near the cathodes increases with time as

$$\sigma(t) = q\mu_e n_e(t) = q\mu_e n_e(0) t^n$$

thus $$I(t) = I_1\ t^n \qquad ---------- (6.25)$$

This mathematical approximation shows that in the early stage of conduction, SCLC may dominate the total leakage current, although the ionically induced current caused by oxygen vacancy migration may also be present. The error for the mathematical time dependence expression of electron concentration, Eqn.(6.23), is caused by the actual change of charge distribution with time shown in Fig.3(b), because the net space charge is not always ideally hyperbolically distributed. In the condition $t < t_o$ Eqn.(6.23) and (6.25) can indicate the tendency of the increase in SCLC following a near power law.

(b) In the succeeding stage of conduction when $t > t_o$, the electric field in the dielectric layer is more likely uniform. In this stage the electronic leakage current is enhanced by oxygen migration, i.e.

$$I(t) = I_2 \, e^{\beta t} \qquad \text{---------- (6.26)}$$

Combining Eqn.(6.25) and (6.26), we obtain

$$I(t) = \begin{cases} I_1 \, t^n & \text{when } t < t_o \\ I_2 \, e^{\beta t} & \text{when } t > t_o \end{cases} \qquad \text{-----(6.27)}$$

From the experimental results of degradation, the leakage current-time characteristics shown in Fig. 27 obey the relation described in Eqn.(6.27) quite well.

For X7R measurements at temperatures lower than 215 ^{o}C and voltages lower than 200 volts, the SCLC phenomenon in the initial stage did not occur sufficiently rapidly for degradation study. On the other hand, at higher temperatures than 300 ^{o}C, both the transition of I-t characteristics from a power law to an exponential law, and the degradation progresses quite rapidly. The temperature dependence of transit time (t_o) characteristic is shown in Fig. 33. It is expected that the transit time decreases exponentially with inverse temperature. This temperature dependence of transit time can be described by

$$t_o = A \exp[\, E/\, kT \,] \qquad \text{---------- (6.28)}$$

where A and E are material dependent constants.

6.2.3 Polarity Effect on Degradation

It has been reported that a Z5U device whose leakage current increased by two orders of magnitude heals back to near its original state when the applied voltage is removed for 20 hours[1]. As indicated in Fig.34, a somehow faster healing effect can be produced by reversing the DC bias polarity. It would take about one hour at 150 ^{o}C and 100 volts for Z5U to heal before degradation reappeared. Considering the observed color gradient[5,6], this is indicative of ionic movement and accumulation which can be repaired to some extent by polarity reversal, with a similar degradation subsequently occurring in the other direction.

In Fig.35 it is seen that a X7R device whose leakage current increases with time heals very rapidly back to near its early state as soon as the bias polarity is reversed. The leakage current suddenly drop to a lower current level. If the "heal back" points (minimum leakage current after polarity reversal) are connected, it may indicates a gradual exponential increase with time as leakage current increases. When the polarity is reversed, the current increases first as power law and then exponentially.

Two interesting phenomena may be noted from the polarity reversal measurements:

(a) The rapid decrease in leakage current indicates the

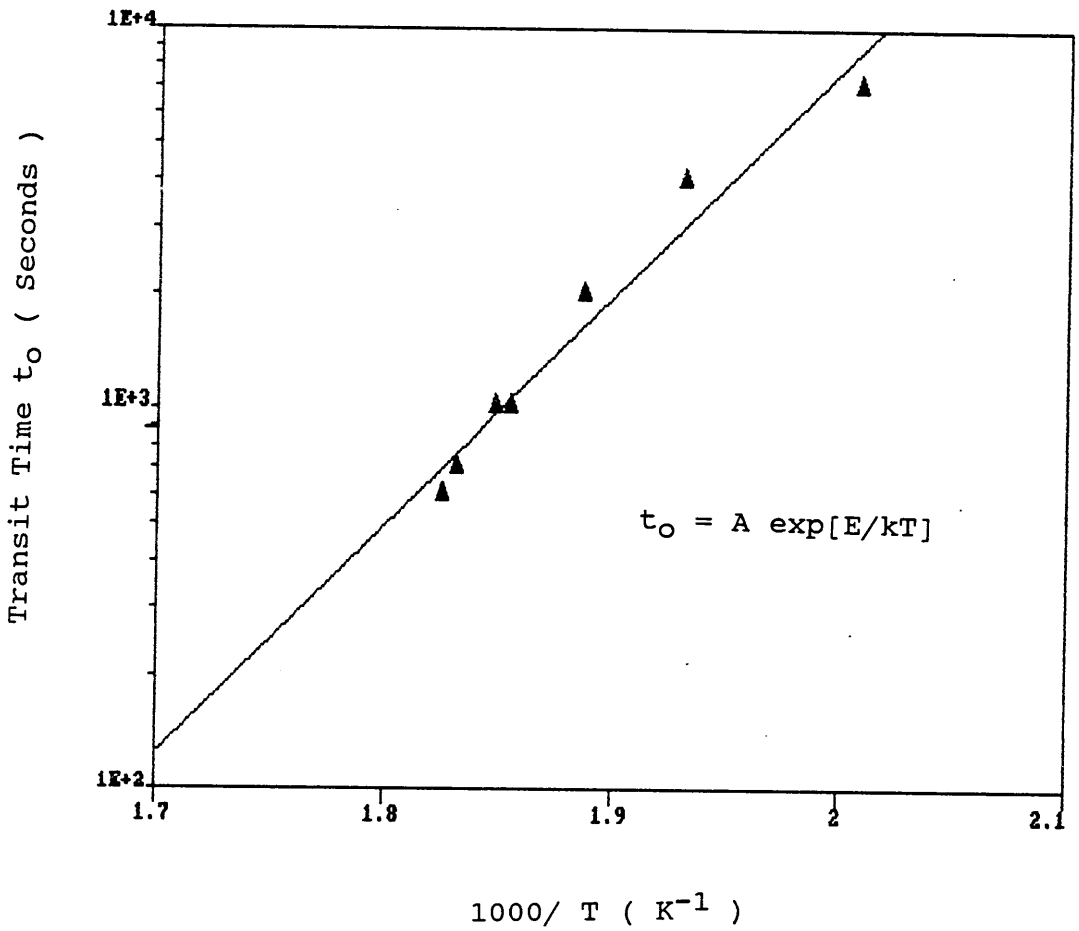

Figure 33. The transit time t_o versus inverse temperature for X7R at V = 200 volts.

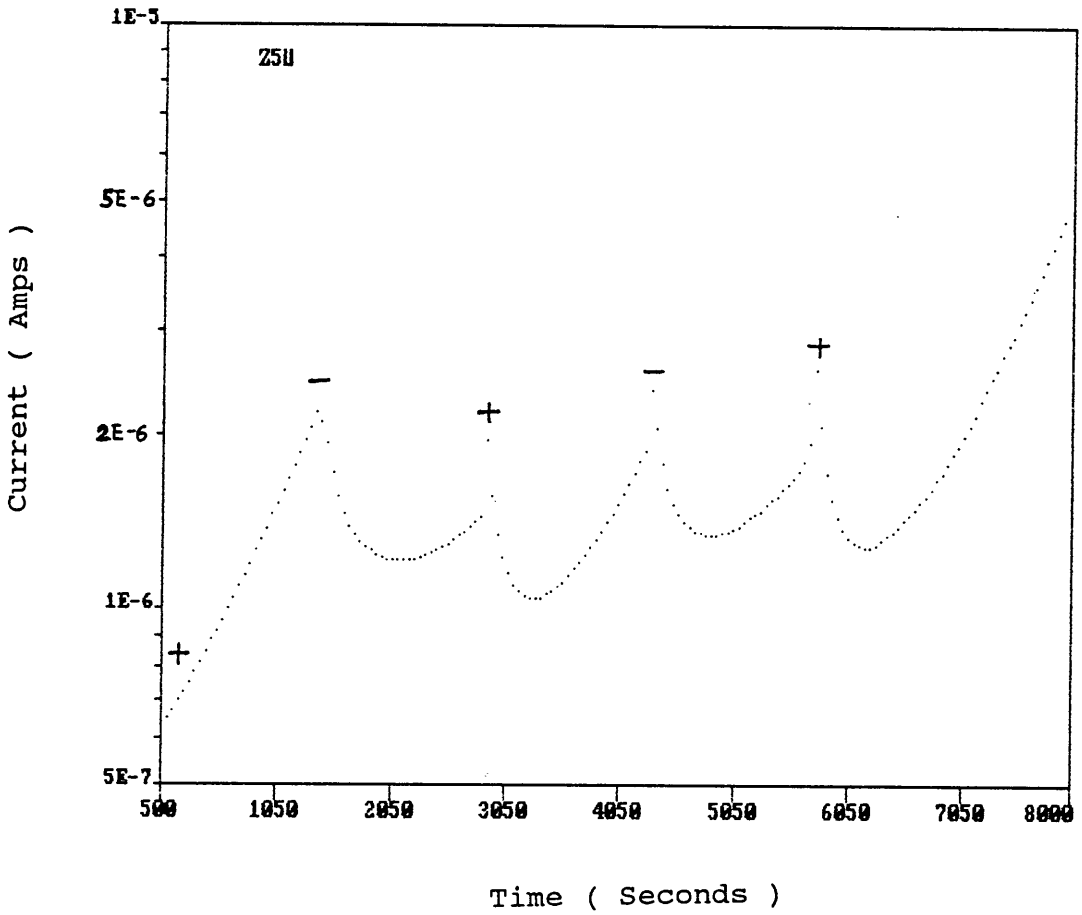

Figure 34. Time dependence of leakage current for Z5U, showing healing effects by reversing the polarity of 100 volts bias at T = 150 ^{o}C.

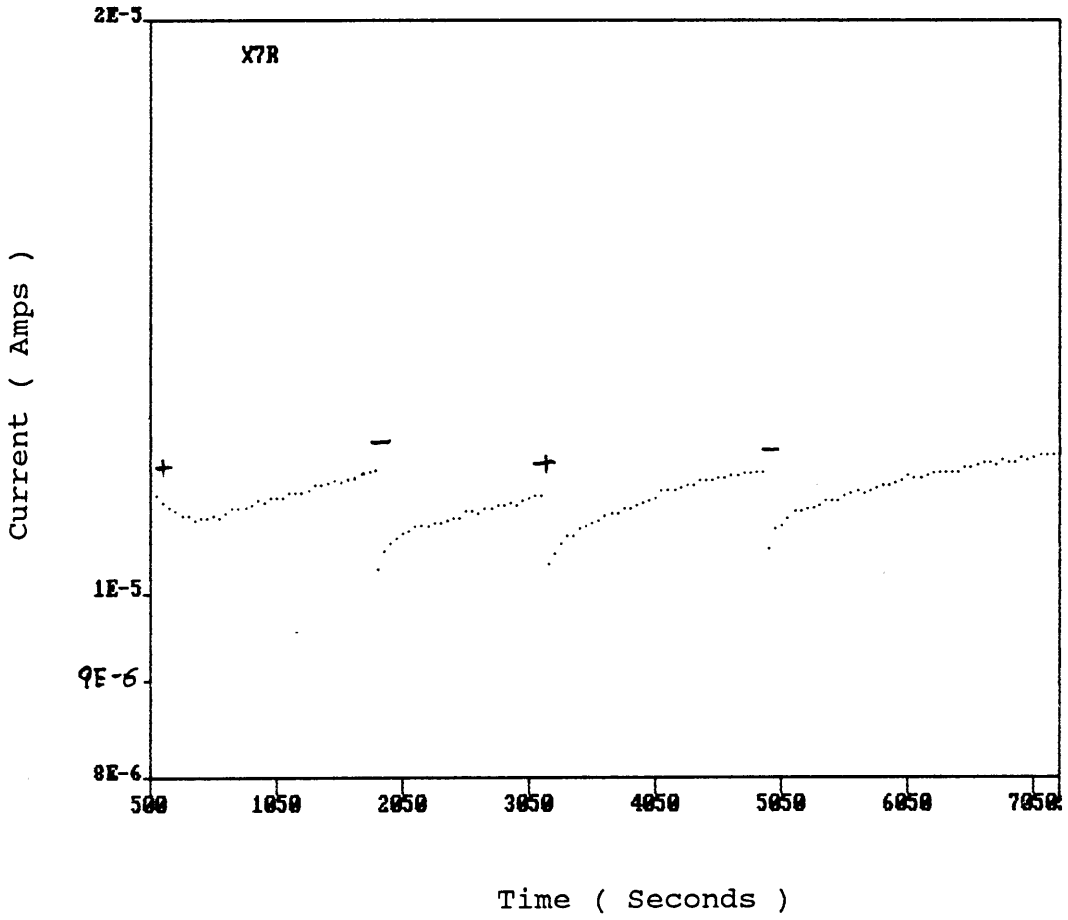

Figure 35. Time dependence of leakage current for X7R at T = 253 °C and 100 volts, showing healing effects by reversing the polarity of 100 volts bias.

healing characteristics of both X7R and Z5U MLC capacitors.

(b) X7R heals much faster than Z5U.

These are quite complicated phenomena that may be due to the processes of electronic or/and ionic motion and accumulation in X7R and Z5U capacitors. It is assumed that the healing process in X7R is more electronic-like while it is more ionic-like process in Z5U. Also,it may be due to the electrode materials used, electrode preparation and the mode of operation.

Chapter 7: CONCLUSIONS AND RECOMMENDATIONS

The main objective of this research was to examine the current transport mechanisms of $BaTiO_3$-based ferroelectric multilayer ceramic capacitors. This was approached mainly through electrical measurements (especially leakage current versus time measurements) under different temperature-voltage stresses. This study has demonstrated how the leakage currents in different types of capacitors change with time, and has provided necessary information leading to the confirmation and development of conduction mechanism models and capacitor degradation characteristics.

Based on the results and discussion in the previous chapter, the findings of this research are summarized below:

(1) The DC leakage currents in ceramic capacitors under low temperature and low voltage stresses are polarization currents that decrease with time in accordance with a power law relation. The polarization current has been ascertained by the results from two independent measurements, i.e. capacitance versus time and discharge current measurements.

(2) The exponent m can be considered as a parameter to related to DC conduction, the frequency dependence of the dielectric constant, and the dielectric loss in the same type of capacitors. The m value is determined by the

material structure and is strongly dependent on temperature. It is, however, only weakly dependent on voltage, and is independent of the dielectric thickness.

(3) Dielectric failure in Z5U and X7R MLC capacitors is proceeded by degradation where the leakage current increases exponentially with time. The degradation rate β is dependent on temperature and voltage.

(4) Capacitor lifetime τ can be described by

$$\tau \propto V^{-n} \exp[E_A/kT]$$

for Z5U MLC capacitors and by

$$\tau \propto \exp[- \alpha V + E_A/kT]$$

for X7R MLC capacitors.

(5) The degradation rate of X7R is much smaller than that of the Z5U. Therefore, it can be concluded that the X7R devices are more stable than the Z5U devices tested.

(6) A charge carrier concentration model, and a reduction of grain boundary barrier height model of degradation have been proposed to explain the

degradation mechanisms in Z5U capacitors.

(7) Anomalous X7R degradation behavior, seen in the power law relation at the initial stage in degradation can be correlated to the effect of space charge limited current. The exponential voltage dependence of the degradation rate may be due to extrinsic defects.

(8) Although the above findings present a clearer picture of the current conduction mechanisms in $BaTiO_3$-based MLC capacitors, it is still necessary to pursue further studies in conduction transport mechanisms. Further research may include the following:

a) Complex impedance measurements at very low frequencies to examine the grain resistance, grain boundary resistance and the metal-dielectric contact resistance.

b) Complex impedance measurements with different DC bias, on a GB resistance dominated capacitor at suitable temperature, to test the effect of the applied bias on the grain boundary resistivity.

c) Degradation measurements on ceramic capacitors of known dielectric thickness to quantify the thickness effect on current and degradation.

d) Activation energy measurements of the samples used for the complex impedance measurements with the same DC bias. This would identify the dominant transport mechanism, such as the grain boundary barrier or hopping potential barrier, or other processes contributing to the activation energy.

e) Complex impedance testing of the samples with different grain sizes while the other parameters and electrode materials are kept the same to understand the grain size effect on electrical conduction.

f) An extensive study, which is most important in capacitor applications, of processing-microstructure-property relationships to obtain a better understanding of the effects of these variables, leading to an optimum control of the device properties.

BIBLIOGRAPHY

1. Hee-Young Lee and Larry C. Burton,"Charge carriers and time dependent currents in $BaTiO_3$-based ceramics",IEEE Tran. on Components, Hybrids and Manuf. Tech., Vol.CHMT -9, No.4, Dec. 1986.

2. H.R.Philipp and L.M.Levinson,"Long-time polarization currents in metal-oxide varistors", J. of Appl. Phys., 47(7), 1976.

3. T.C.Chapman and H.J.Wintle,"Dielectric absorption currents and surface charge on polymeric insulators", J. Appl. Phys. 51(9) 1980.

4. A.K.Jonscher,"Dielectric relaxation in solids", Chelsea Dielectrics Press Ltd., London, 1983.

5. J.N.Schunke,"Intrinsic degradation mechanisms of barium titanate based multilayer ceramic capacitor", M.S. Thesis, VPI&SU, 1985.

6. Hee-Young Lee,Kyo-Chol Lee,J.N.Schunke and L.C.Burton, "Leakage currents in multilayer ceramic capacitors", IEEE Tran. on Compon., Hybrids and Manuf. Tech., Vol.CHMT-7, No.4, Dec. 1984.

7. L.C.Burton,"Intrinsic mechanisms of multilayer ceramic capacitor failure", Annual Report to ONR Contract No. N00014-83-K-0168, April 1986.

8. A.K.Jonscher,"Hopping loss in polarisable dielectric media", Nature, Vol.250, pp.191, July 1974.

9. A.K.Jonscher,"Physical basis of dielectric loss", Nature, Vol.253, pp.717, Feb. 1975.

10. L.C.Burton,"Voltage dependence of activation energy for multilayer ceramic capacitors", IEEE Tran. on Compon., Hybrids, and Manuf. Tech., Vol.CHMT-8, No.4, Dec. 1985.

11. AVX Corp.,"The capacitor", Technical Information.

12. S.S.Villamil,"Impedance characteristics and grain boundary effects in barium titanate -based multilayer capacitors", M.S. Thesis, VPI&SU, 1987.

13. M.Kahn,"Technical Information-m aterials and manufacture" AVX Corp., Myrtle Beach, S.C.

14. J.M.Herbert,"Ceramic dielectrics and capacitors", G&B Science Publishers, 1985.

15. I.K.Yoo,L.C.Burton and F.W.Stephenson,"Electrical conduction mechanisms of barium titanate-based thick-film capacitors", IEEE Tran. on Compon., Hybrids, and Manuf. Tech., Vol.CHMT-10, No.2, June 1987.

16. W.A.Schultze,L.E.Cross and W.R.Buessem,"Degradation of $BaTiO_3$ ceramic under high ac electric field", J. Amer. Ceram. Soc., Vol.63, pp.83, 1980.

17. W.J.Minford,"Accelerated life testing and reliability of high K multilayer ceramic capacitors", IEEE Tran. on Compon., Hybrids, and Manuf. Tech., Vol.CHMT-5, No.3, pp.297, 1982.

18. H.B.Haanstra and H.Ihrig,"Voltage contrast imaging of PTC-type $BaTiO_3$ ceramics having low and high titanate excess", Phys. Stat. Sol., (a)39, K7, 1977.

19. E.Scholl,"Lowering of grain-boundary barrier heights by grain curvature", J. Appl. Phys. 60(4), pp.1434, 1986.

20. W.Heywany,"Semiconducting barium titanate", J. Mater. Sci., Vol.6, pp.1214, 1971.

21. K.Bai,Byoung-Chul Shin and Ho-Gi Kim,"Grain size effect on ac degradation of barium titanate ceramics",(to be published)

22. W.G.Morris,"Physical properties of the electrical barriers in varistors", J. Vac. Sci. Technol., Vol.13, No.4, pp.926, 1976.

23. P.L.Hower and T.K.Gupta,"A barrier model for ZnO varistors", J. Appl. Phys.,50(7), pp.4847, 1979.

24. P.Gerthsen and B.Hoffman,"Current-voltage characteristics and capacitance of single grain boundaries in semiconducting $BaTiO_3$ ceramics", Solid-state Electronics, Vol.16, pp.617, 1973.

25. H.Ihrig and W.Puschert,"A systematic experimental and theoretical investigation of the grain-boundary resistivities of n-based $BaTiO_3$ ceramics", J. Appl. Phys., 48(7), 1977.

26. T.M.Berlicki,"Voltage degradation model of thin film cepecitors",Active and passive Elc. Comp., Vol.12, pp.63, 1985.

27. B.S.Rawal and N.H.Chan,"Conduction and failure mechanisms in barium titanate based ceramics under highly accelerated conditions",Proc. 34th Electronic Component Conf., pp.184, 1984.

28. E.Loh,"Development of a model for voltage degradation of various dielectric materials", IEEE Tran. on Compon., Hybrids, and Manuf. Tech., Vol.CHMT-4, No.4,pp.536,1981.

29. J.Daniels and R.Wernicke,"New aspects of a improved PTC model", Philips Res. Rep., 31, pp.544, 1976.

30. R.Waser,"Accelerated life testing and long-term reliability of multilayer ceramic capacitors", to be published.

31. P.Salomon,M.Klein and M.Albert,"A statistical model for step and ramp voltage breakdown tests in thin insulators", Thin Solid Film, 35, pp.321, 1976.

32. K.Eda,A.Iga and M.Matsuoka,"Degradation mechanism of non-Ohmic zinc oxide ceramics", J. Appl. Phys., 51(5), pp.2678, 1980.

33. T.K.Gupta,W.G.Carlson and P.L.Hower,"Current instability phenomena in ZnO varistors under a continuous ac stress", J. Appl. Phys., 52(6), pp.4104, 1981.

34. F.S.Fisher,"Failure characteristics of thin film capacitors", Proc. 10th Annu. IEEE Int. Rel. Phys. Symp. pp.183, 1972.

35. D.D.Glower and R.C.Hechman,"Conduction-ionic or electronic-in $BaTiO_3$", J. Chem. Phys., Vol.41, pp.877, 1964.

36. M.K.Paria, H.S.Maiti,"Electrical conduction in barium titanate", J. Mater. Sci. Letter, (3), pp.578, 1984.

37. D.L.Ridpath, D.A.Wright,"Electrical conductivity of reduced barium titanate crystals", J. Mater. Sci.,5, pp.487, 1970.

38. H. Ihrig,"On the polaron nature of the charge transport in $BaTiO_3$", J. Phys. C: Solid state Phys., 9, pp.3469, 1975.

39. R.Stumpe,D.W.Wagner and D.Bauerle,"Influence of bulk and interface properties on the electric transport in ABO_3 perovskites", Phys. Stat. Sol.,(a) 75, pp.143, 1983.

40. H.Y.Lee,"Electrical Transport properties of barium titanate-based capacitor ceramics", Ph.D.Thesis, VPI&SU, 1987.

41. L.Benguigui,"Space charge limited currents in $BaTiO_3$ single crystals", Solid State Communications, Vol.7, No.17, pp.1245, 1969.

42. A.Branwood, O.H.Hughes, J.D.Hurd and R.H.Tredgold, "Evidence for space charge conduction in barium titanate single crystals", Proc. Phys. Soc., Vol.79, pp.1161, 1962.

43. Y.V.Zabara,A.Y.Kudzin and K.A.Kolesnichenko,"Space-charge-limited currents in barium titanate single crystals", Phys. Stat. Sol.(a), Vol.38, pp.131, 1976.

44. L.Benguigui,"Electrical phenomena in barium titanate ceramics", J. Phys. Chem. Solids, 34(4), pp.573, 1973.

45. K.Lehovec and G.A.Shirn,"Conductivity injection and extraction in polycrystalline barium titanate", J. Appl. Phys., 33(6), pp.2036, 1962.

46. Y.Goto and S.Kachi,"Studies on the mechanism of electric conduction in Fe-doped $BaTiO_3$ single crystals by applying Kerr effect", J. Phys. Chem. Solids, Vol.32, pp.889, 1971.

47. A.Steinbrunn,H.Reteno and J.C.Colson,"Experimental study of MoO_3 electrical conductivity changes under low oxygen pressures", in 'Transpt. Nonstoichiometric Compounds',G. Simkovich and V.S.Stubican, edt., NATO ASI Series, Vol.129, 1984.

48. I.Bunget and M.Popescu,"Physics of solid dielectrics", Materials Sci. Monographs 19, Elsevier Pub., 1984.

49. R.Coelho,"Physics of dielectrics for the engineer", Sci. Pub. Company, 1979.

50. A.K.Jonscher,"A many-body universal approach to dielectric relaxation in solids", H.L.Goodman Edt. pp.22-45, 1980.

51. G.E.Pike and C.H.Seager,"The DC voltage dependence of semiconductor grain boundary resistance", J. Appl. Phys. 50, pp.3414, 1979.

52. G.Blatter and G.Greuter,"Electrical properties of grain boundaries in the presence of deep bulk traps", 'Polycrystalline Semiconductors', edt. by G,Harbeke,

Springer Verlag, 1985.

53. C.Schaffrin,"Oxygen diffusion in $BaTiO_3$ ceramics", Phys. Stat. Sol.,(a)35, pp.79, 1976.

54. J.D.Keck,"Electrical degradation of high purity barium titanate", Ph.D.Thesis, Univ. of Missouri-Rolla, 1976.

55. C.H.Seager and G.E.Pike,"Grain boundary states and varistor behavior in silicon bicrystals", Appl. Phys. Lett. Vol.35, pp.709, 1979.

56. H.J.Leamy and G.E.Pike,"Grain boundaries in semiconductors", H.Seager, edt. Amsterdam, The Netherlands, North Holland, 1982.

57. H.D.Park and D.A.Payne,"Characterization of internal boundary layer capacitors", in 'Grain Boundary Phenomena in Electronic Ceramics', Amer. Ceram. Soc., pp.242, 1981.

58. G.Goodman,"Capacitors based on ceramic grain boundary barrier layer- a view", in 'Grain Boundary Phenomena in Electronic Ceramics', Ammer. Ceram. Soc., pp.215, 1981.

59. H.Nemoto and I.Oda,"Direct examination of PTC action of single grain boundaries in semiconducting $BaTiO_3$ ceramics", J. Amer. Ceram. Soc., Vol.63, pp.398, 1980.

60. K.Eda,"Conduction mechanism of non-Ohmic zinc oxide ceramics", J. Appl. Phys., 45(5), pp.2964, 1978.

61. L.M.Levinson and H.R.Philipp,"The physics of metal oxide varistors", J. Appl. Phys., 46(3), pp.1332, 1975.

62. P.L.Hower and T.K.Gupta,"A barrier model for ZnO varistors", J. Appl. Phys., 50(7), 1979.

63. L.L.Kazmerski, Ed.,"Polycrystalline and amorphous thin films and devices", New York, Academic, 1980.

64. M.Kuwabara,"Determination of the potential barrier height in barium titanate ceramics", Solid-state Electronics, 27, pp.929, 1984.

65. L.C.Burton,"Intrinsic mechanisms for multilayer ceramic capacitor failure", ONR Anuual Report, April 1985.

66. W.D.Kingery, H.K.Bowen and D.R.Uhlmann,"Introduction to ceramics", John Wiley & Sons, 1976.

67. W.Heywang,"Resistivity anomaly in doped barium

titanate", J. Amer. Ceram. Soc., Vol.47, pp.484, 1976.

68. M.Kahn,"Effects of sintering and grain growth reactions on the distribution of niobium additives in barium titanate ceramics", Pen. State Univ., 1969.

69. L.C.Burton,"Models for electronic conduction across ceramics grain boundaries", Paper presented at Mate. Res. Soc., Fall meeting, Boston. MA, 1985.

70. K.Okazaki and H.Igarashi,"Processing-property relations in dielectric capacitors", Ferroelectrics, Vol.27, pp.263, 1980.

71. M.A.Lampert and P.Mark,"Current injection in Solids", New York, Academic, 1970.

72. M.A.Lampert and R.B.Schilling,"Current injection in solids: the regional approximation method", in 'Semiconductors and Semimetals", Vol.6, R.K.Willardson and A.C.Beer eds., Academic Press, 1970.

73. E.Loh,"A model of DC leakage in ceramic capacitors", J. Appl. Phys., 53(9), pp.6229, 1982.

74. Y.K.Sharma, R.N.Sharma and V.S.Raghav,"Current injection in an insulator with specially distributed shallow traps", J. Appl. Phys., 54(7), pp.4213, 1983.

75. N.Koda,"Space-charge-limited currents in insulators with shallow traps and conductivity distribution", Japn. J. Appl. Phys., Vol.26, pp182, 1987.

76. H.Bottger and V.V.Brybsin,"Hopping conduction in solids", VCH Pub., 1985.

77. C.Kittel,"Introduction to Solid State Physics", 6th edt., John Wiley & Sons Inc., 1986.

78. G.Goodman,"Ceramic capacitor materials", in 'Ceramic Materials for Electronics',R.C.Buchanan edt., Marcel Dekker, Inc., 1986.

79. F.F.Mazda,"Discrete Electronic Components", Cambridge Univ. Press, 1981.

80. V.V.Daniel,"Dielectric relaxation", Academic Press, Inc., 1967.

The vita has been removed from the scanned document